THE JOURNAL OF BIOLOGICAL CHEMISTRY VOL. 287, NO. 42, pp. 35299–35317, October 12, 2012

A Subunit of Eukaryotic Translation Initiation Factor 2α-Phosphatase (CreP/PPP1R15B) Regulates Membrane Traffic*[S]

Received for publication, May 10, 2012, and in revised form, August 17, 2012 Published, JBC Papers in Press, August 22, 2012, DOI 10.1074/jbc.M112.379883

Nicole Kloft[‡], Claudia Neukirch[‡], Gisela von Hoven[‡], Wiesia Bobkiewicz[‡], Silvia Weis[‡], Klaus Boller[§], and Matthias Husmann[‡1]

From the [‡]Institute of Medical Microbiology and Hygiene, University Medical Center, Johannes Gutenberg-University Mainz, Hochhaus am Augustusplatz, 55131 Mainz, Germany and the [§]Department of Immunology, Morphology Section, Paul Ehrlich-Institute, 63225 Langen, Germany

Background: The constitutive reverter of eIF2α phosphorylation (CReP/PPP1r15B) targets the catalytic subunit of protein phosphatase 1 (PP1c) to p-eIF2α to promote translation initiation.
Results: CReP associates with membranes and regulates membrane traffic in a PP1c-independent manner.
Conclusion: CReP is co-opted by the traffic machinery.
Significance: The data reveal a novel link between the molecular machineries regulating translation and traffic.

The constitutive reverter of eIF2α phosphorylation (CReP)/PPP1r15B targets the catalytic subunit of protein phosphatase 1 (PP1c) to phosphorylated eIF2α (p-eIF2α) to promote its dephosphorylation and translation initiation. Here, we report a novel role and mode of action of CReP. We found that CReP regulates uptake of the pore-forming *Staphylococcus aureus* α-toxin by epithelial cells. This function was independent of PP1c and translation, although p-eIF2α was involved. The latter accumulated at sites of toxin attack and appeared conjointly with α-toxin in early endosomes. CReP localized to membranes, interacted with phosphomimetic eIF2α, and, upon overexpression, induced and decorated a population of intracellular vesicles, characterized by accumulation of N-(lissamine rhodamine B sulfonyl)phosphatidylethanolamine (N-Rh-PE), a lipid marker of exosomes and intralumenal vesicles of multivesicular bodies. By truncation analysis, we delineated the CReP vesicle induction/association region, which comprises an amphipathic α-helix and is distinct from the PP1c interaction domain. CReP was also required for exocytosis from erythroleukemia cells and thus appears to play a broader role in membrane traffic. In summary, the mammalian traffic machinery co-opts p-eIF2α and CReP, regulators of translation initiation.

Phosphorylation of eukaryotic translation initiation factor 2 α (eIF2α)[2] at Ser-51 is a conserved cellular response to stress, which leads to attenuation of global translation and overexpression of select genes (1). This so-called integrated stress response serves multiple adaptive functions (2). Levels of Ser-51-phosphorylated eIF2α (p-eIF2α) are controlled through both phosphorylation and dephosphorylation. In mammalian cells, four eIF2α kinases are known, which respond to different types of stress (2). Dephosphorylation of p-eIF2α is mediated by the catalytic subunit of protein phosphatase 1 (PP1c) in complex with either of two regulatory subunits (PPP1r15A or -B), known as GADD34 (growth arrest and DNA damage 34) and CReP (constitutive reverter of eIF2α phosphorylation), respectively. GADD34 expression is induced upon stress in a p-eIF2α-dependent manner to restart global translation after stress (3). In contrast, CReP is expressed in unstressed cells. Whereas GADD34 knock-out mice appear normal, GADD34/CReP double knock-out mice do not survive gestation. The sole indispensable function of CReP during mammalian development is thought to be dephosphorylation of eIF2α, but rescue of fetal anemia in CReP knock-out mice by the S51A mutation of eIF2α was incomplete (4). Knockdown (KD) of CReP expression with siRNAs or treatment with salubrinal (SAL), a selective inhibitor of eIF2α dephosphorylation (5), was reported to promote survival of stressed cells (6). However, sustained eIF2α phosphorylation may also exert deleterious effects (7).

Membrane damage caused by agents like pore-forming toxins (PFT) or mechanical force represents an archetypal form of stress. Various signaling pathways of potential relevance to the defense against PFT have been identified (8–21). Membrane traffic is critically involved in defenses against PFT (22–25) or other membrane-damaging agents or forces (26–34). Comparison of the response to various toxins forming pores of different diameters indicated that pro-survival signaling involves both conserved (10), and divergent pathways (10, 13, 35). Similarly,

* This work was supported by Deutsche Forschungsgemeinschaft, CRC 490, Project D3 (to M. H.). The contributions of G. v. H. were in partial fulfillment of her thesis requirements.
[S] This article contains supplemental Movies 1–4.
[1] To whom correspondence should be addressed: Institute of Medical Microbiology and Hygiene, University Medical Center, Johannes Gutenberg-University Mainz, Hochhaus am Augustusplatz, 55131 Mainz, Germany. Tel.: 49-6131-179364; Fax: 49-6131-179234; E-mail: husmann@uni-mainz.de.
[2] The abbreviations used are: eIF2α, eukaryotic translation initiation factor 2α; p-eIF2α, phosphorylated eIF2α; PP1c, protein phosphatase 1 catalytic subunit; KD, knockdown; SAL, salubrinal; PFT, pore-forming toxins; PM, plasma membrane; EGFP, enhanced green fluorescent protein; CHX, cyclohexamide; PAL, palytoxin; IP, immunoprecipitation; AChE, acetylcholine esterase; IF, immunofluorescence; NP, NeutrAvidin pull-down; VDC, vesicles decorated with CReP; TrfR, transferrin receptors; MVB, multivesicular bodies; ER, endoplasmic reticulum.

specifics of membrane traffic during repair may depend on the membrane-damaging agent (22–25, 27).

The small β-barrel pore forming α-toxin is an important virulence factor of *Staphylococcus aureus*, (36, 37). It is secreted as a 34-kDa monomeric protein, which, upon binding to susceptible target cells, forms a heptameric transmembrane pore (7-mer) with an inner diameter of ~1.5 nm (38). Various proteins and lipids have been implicated in binding, oligomerization of α-toxin, and membrane perforation by this pore former (39–42). The membrane-inserted 7-mer is remarkably resistant to SDS and proteolysis (43), allowing it to be accurately traced after binding to cells (25). We found that cells remove α-toxin pore complexes from their plasma membrane (PM) by endocytosis (25) and also that the dramatic ATP loss following perforation is contained by a vital autophagic response, which depends on phosphorylation of eIF2α (44).

In this context, we became interested in the role of eIF2α *dephosphorylation* for the cellular response to α-toxin. The fact that inhibition or silencing of CReP aggravated energy loss in target cells of α-toxin prompted us to investigate the underlying mechanism. Ultimately, this led to the discovery that CReP impacts membrane traffic and that it does so in a PP1c-independent fashion.

EXPERIMENTAL PROCEDURES

Antibodies, Plasmids, and Chemicals—Antibodies against p-eIF2α and eIF2α were from Abcam (immunofluorescence) and Cell Signaling Technology (Western blot). Antibodies against GADD34, Nck1/2, histone H1, vimentin, PP1c, CD71 (for Western blot), and acetylcholine esterase (AChE) were purchased from Santa Cruz Biotechnology, Inc. (Santa Cruz, CA). Anti-PPP1R15B, -E-cadherin, -β-actin, and -Hsp90 were from the Proteintech Group, Monosan, Sigma, and StressMarq, respectively. Anti-human CD71-FITC was from eBioscience, and Alexa-Fluor®-conjugated and HRP-conjugated secondary antibodies were from Molecular Probes and Cell Signaling Technology. Plasmid encoding human CReP was purchased from imaGenes, and CReP cDNA was subcloned into p3xFLAG-CMV-10 (Sigma), EGFP-C1, or dsRed-C1 (Clontech). EGFP-tagged, truncated versions of CReP were made by PCR amplification of the respective fragments and subcloning into pEGFP-C1. pEGFP-eIF2α, pEGFP-eIF2αS51A, and pEGFP-eIF2αS51D were generated by excision of the corresponding cDNAs from pCDNA3-CD2-eIF2αwt or the corresponding plasmids carrying the mutant versions of eIF2α, obtained from Addgene (plasmids 21807–21809; Dr. David Ron), and cloning into pEGFP-C1 (Clontech). pEGFP-eIF2αS51D-NTD and pEGFP-eIF2α-CTD encode the EGFP-tagged N-terminal domain of eIF2αS51D and the EGFP-tagged C terminus of eIF2α, respectively; these plasmids were made by PCR amplification of the N- or C-terminal halves of EGFP-eIF2αS51D, TA cloning into pGEM-T (Promega), and subcloning into pEGFP-C1. The plasmids pEGFP-Rab5Q79L and pEGFP-Rab5wt were kindly provided by Dr. Marino Zerial. The following small interfering RNAs and control siRNA were from Qiagen: PPP1R15B 1, 5′-AAGGGAUGGAUGCAGGUUCCA-3′ (6); PPP1R15B 2, 5′-CCGAAUAAGUGUAGUUGAUUA-3′; eIF2α-5, 5′-GGCUGUAAAUCCUAGACUUTT-3′; eIF2α-7, 5′-GGCGUAUCCGUUCUAUCAATT-3′; GCN2, 5′-CAAGGUUAAGUCUUUCGAGAA-3′. PP1c-siRNA (sc-36299) was from Santa Cruz Biotechnology, Inc.; PKR-siRNA (5′-GACGGAAAGACUUACGUUATT-3′) was from Ambion. SAL, cyclohexamide (CHX), and palytoxin (PAL) were obtained from Calbiochem; chloramphenicol was from Sigma. *S. aureus* α-toxin and radiolabeled and fluorescently labeled α-toxin were made as published (25, 44).

Cells, Culture and Treatment Conditions, and Transfections—Culture, toxin treatment, and transfection of non-virally transformed human keratinocytes, HaCaT, were as described (25, 44). In brief, HaCaT cells, non-virally transformed human keratinocytes (45), were grown in DMEM with 10% fetal calf serum in a humidified incubator with 5% CO_2. Normal human epithelial keratinocytes (PromoCell) were grown in keratinocyte growth medium 2 (PromoCell), and experiments were carried out with cells in the third and fourth passages. Unless stated otherwise, subconfluent grown HaCaT cells were loaded with 1 μg/ml α-toxin (or 2 μg in the case of fluorescently labeled toxin) at 4 °C for 40 min, washed, and incubated at 37 °C for various times. Inhibitors were added 1 h prior to toxin loading and were present throughout the experiments. For uptake studies with internally radiolabeled or fluorescently labeled α-toxin, cells were loaded at 4 °C with 1 or 2 μg/ml α-toxin, respectively. Although at 37 °C, the permanent presence of toxin at these doses would kill HaCaT cells, this is not the case at 4 °C; under these conditions, toxin binds to the cell surface without forming pores. Before shifting toxin-loaded cells to 37 °C, cells were washed to eliminate unbound toxin. Shifting toxin-loaded cells to 37 °C leads to a pronounced drop of cellular ATP, but levels return to normal within hours, and cells remain viable. Assays for intracellular ATP were performed as described elsewhere (46).

Red Blood Cell Lysis Assay—Rabbit erythrocytes in PBS containing 1% BSA were incubated with α-toxin at various concentrations in the presence or absence of 40 μM salubrinal for 30 min at 37 °C. After centrifugation, supernatants were transferred to 96-well plates, and hemoglobin release was measured at $A_{415\,nm}$.

Experiments with K562 Cells—K562 cells (human erythromyeloblastoid leukemia cell line; ACC-10; DSMZ), transfected with control siRNA, PP1 siRNA, or CReP siRNA for 48 h, were incubated in 10 ml of RPMI medium with 10% FBS (Invitrogen) at 37 °C for 24 h.

Transient Transfection—Cells were transfected with double-stranded siRNAs by using the AMAXA system (Lonza) according to the manufacturer's protocol. Transfection of plasmids was done with jetPEI™ (Polyplus transfection SA) as recommended by the supplier. Small interfering RNA for PPP1R15B was as published (6).

Metabolic Labeling of Nascent Proteins—Incorporation of L-[^{35}S]methionine into proteins was determined as described (47). HaCaT cells were seeded at a density of 3.5×10^5 cells/well into 6-well plates. Cells were treated with 100 ng/ml α-toxin in DMEM plus 10% FBS for 1 h and were starved in DMEM lacking methionine (Invitrogen). After 15 min, cells were pulse-labeled with L-[^{35}S]methionine at a concentration of 10 μCi/well for 30 min, and after incubation for 1 h at 37 °C, cells were

washed and analyzed for incorporation of the label or incubated in toxin-free medium for an additional 3 h prior to analysis. To detect newly synthesized proteins by fluorescence microscopy, we employed bioorthogonal noncanonical amino acid tagging (48); metabolic labeling with L-azidohomoalanine and alkyne-based fluorescent labeling of nascent proteins were performed as detailed in the protocols of the Click-IT® kit (Invitrogen).

Western Blots—For Western blots, cell lysates were mixed with 2× SDS-loading buffer (10% (v/v) glycerol, 5% (v/v) 2-mercaptoethanol, 2% (w/v) SDS, and bromphenol blue) and boiled for 5 min at 95 °C. Proteins were separated by SDS-PAGE (10%) and electroblotted onto nitrocellulose membrane. After blocking for 1 h at room temperature in 5% BSA (w/v) or 5% skim milk (w/v) in TBST, membrane was incubated with first antibody overnight at 4 °C, washed three times in TBST, and incubated with HRP-conjugated second antibody for 1 h at room temperature. After three washing steps, bound antibody was detected by ECL (Roche Applied Science). Intensity of bands was measured using ImageJ software (National Institutes of Health; W. S. Rasband, 1997–2011).

(Co-)Immunoprecipitation—Two types of co-IP experiments were performed. First, antibodies against p-eIF2α, CReP, or GFP were used to co-immunoprecipitate radiolabeled α-toxin from lysates of treated cells; in a second approach, immobilized anti-EGFP was used to test whether radiolabeled toxin co-isolates together with EGFP fusion proteins from lysates of transfected cells. For co-IP of α-toxin, cells were loaded with [^{35}S]methionine-labeled α-toxin (1 μg/ml) for 40 min at 4 °C. Unbound α-toxin was removed by two washing steps with ice-cold PBS, DMEM was added, and cultures were incubated for 10 and 20 min at 37 °C. Cells were washed, harvested by using a cell scraper, and collected by centrifugation. The cell pellet was lysed in lysis buffer (50 mM Tris-Cl, pH 7.4, 300 mM NaCl, 2% Nonidet P-40, protease inhibitor mixture (Roche Applied Science), and phosphatase inhibitor mixture (Roche Applied Science)) and precleared by incubation with Protein A/G-agarose (Santa Cruz Biotechnology, Inc.) at 4 °C for 3 h. The lysate was divided into four aliquots; 1 μg of rabbit antibody against α-toxin (Sigma), phospho-eIF2α (Cell Signaling Technology), PPP1R15B (Proteintech Group), or control rabbit antibody was added to each aliquot; and the mixtures were incubated for 2 h at 4 °C. After the addition of Protein A/G-agarose and incubation overnight at 4 °C, immunocomplexes were washed and eluted from agarose beads by incubation in Laemmli buffer without β-mercaptoethanol for 10 min at 50 °C; aliquots were combined. Monomers and SDS-stable 7-mers were separated by electrophoresis and detected by fluorography. For experiments involving IP of EGFP-tagged proteins (wild type, mutated, truncated eIF2α; wild type CReP), the respective EGFP fusion proteins were transiently expressed in HaCaT cells. Lysates were obtained and subjected to IP with immobilized monoclonal anti-GFP according to the supplier (GFP-tagged protein isolation kit, Miltenyi Biotec); CReP was detected by Western blot; and [^{35}S]methionine-labeled α-toxin was detected by fluorography.

Differential Detergent Lysis—Differential detergent lysis was performed with the subcellular proteome extraction kit (S-PEK) from Millipore according to the protocol of the supplier.

Sequential Neutravidin Pull-down/Immunoprecipitation—To analyze toxin-dependent association of p-eIF2α with the PM, cells were treated with unlabeled α-toxin and subsequently surface-biotinylated with EZ®-Link sulfosuccinimidyl 2-(biotinamido)-ethyl-1,3-dithiopropionate (Thermo Scientific), and lysates were subjected to affinity purification with NeutrAvidin agarose resin according to protocols provided by the supplier (Thermo Scientific). The precipitated material was dissolved in SDS-loading buffer and analyzed by Western blot; bands were quantified by densitometry using ImageJ. For semiquantitative detection of changes of surface-exposed or internalized α-toxin, cells were loaded with internally [^{35}S]methionine-labeled α-toxin (1 μg/ml), incubated for various times, and surface-biotinylated with EZ®-Link sulfosuccinimidyl 2-(biotinamido)-ethyl-1,3-dithiopropionate. Labeled surface proteins were affinity-purified with NeutrAvidin agarose resin. Non-biotinylated α-toxin in the flow-through was immunoprecipitated with antibodies against α-toxin (Sigma). SDS-stable α-toxin 7-mers were separated from α-toxin monomers by electrophoresis, detected by fluorography, and quantified by liquid scintillation counting (25).

Exosome Preparation and AChE Assay—Supernatants of K562 cells were centrifuged at 10,000 × *g* to remove cell debris and subsequently at 100,000 × *g* for 2 h at 4 °C to collect exosomes, which were washed with PBS and finally resuspended in 100 μl of PBS. An acetylcholinesterase activity assay was performed as described (49). A 50-μl exosome fraction and 200 μl of 1.25 mM acetylthiocholine iodide, 0.1 mM 5,5-dithio-bis(2-nitrobenzoic acid) (Sigma) in PBS were prewarmed for 10 min at 37 °C. Both solutions were mixed, and changes in absorption at 450 nm were measured at room temperature for 1 h with a plate reader spectrophotometer.

Flow Cytometry—Cells were harvested by centrifugation at 800 × *g* for 5 min, and pellets were washed with PBS, fixed with 2% paraformaldehyde, and incubated with FITC-coupled anti-human CD71 antibody (eBioscience) for 1 h at room temperature in the dark. After two washing steps with PBS, cells were analyzed using a FACScan flow cytometer (BD Biosciences) and CellQuest software; 10,000 cells were analyzed per run.

Immunofluorescence (IF) Microscopy—Cells grown on glass coverslips were fixed with 2% paraformaldehyde in PBS for 10 min at room temperature and permeabilized with 0.1% Triton X-100 for 10 min. Indirect immunofluorescence staining was performed with Alexa488-, Alexa647-, or Alexa594-conjugated secondary antibodies, and coverslips were mounted on slides using Fluoroprep (bioMérieux® SA). Confocal images were captured with a Zeiss 510Meta microscope equipped with a Plan-Apochromat 63×/1.4 numerical aperture oil objective. Wide field microscopy was carried out with a Zeiss Axiovert 200 M epifluorescence microscope and a Plan-Apochromat 100×/1.4 numerical aperture oil objective. Epifluorescence microscopy digital images were acquired with a Zeiss Axiocam; iterative deconvolution of *z*-stacks and colocalization analyses were performed with tools of Axiovision and Metamorph software; further image processing was done with Axiovision software and Adobe Photoshop. To evaluate juxtaposition of total

membrane-bound toxin and p-eIF2α, the fraction of pixels corresponding to total membrane-bound α-toxin expected to be juxtaposed by chance to p-eIF2α in planes z2 through z6 was calculated and compared with the actual overlap. The colocalization tool of Axiovision was employed with automatic thresholding to generate dot plots and to determine Pearson's correlation coefficient.

Replicates and Statistical Analysis—Unless stated otherwise, data displayed are from ≥3 independent experiments. Student's *t* test was employed to assess statistical significance of differences between mean values. Significance was assumed at $p < 0.05$.

RESULTS

A Translation-independent Function of CReP—Previously, we found that α-toxin causes rapid phosphorylation of eIF2α in a human keratinocyte cell line, HaCaT (44). This response is concentration-dependent (Fig. 1*A*) and is not observed with pore dead mutant D152C that still binds to cells (Fig. 1*B*). SAL, an inhibitor of eIF2α-phosphatase, enhances phosphorylation of eIF2α in α-toxin-treated cells (Fig. 1*C*). To examine a potential effect on the metabolic recovery from membrane perforation by *S. aureus* α-toxin, we assessed the effect of SAL on toxin-loaded cells. The characteristic course of ATP loss and recovery after α-toxin attack was altered in the presence of the eIF2α dephosphorylation inhibitor, in that initial ATP loss was slightly enhanced, and recovery was markedly inhibited (Fig. 1*D*). In striking contrast to SAL, CHX neither prevented replenishment of ATP nor mitigated the adverse effect of SAL (Fig. 1*E*). SAL did not increase hemolytic power or heptamer formation (Fig. 1, *F* and *G*). The efficacy of the treatments (SAL and CHX) was verified by metabolic labeling. Predictably, CHX prevented [^{35}S]methionine incorporation into newly synthesized proteins (Fig. 1*H*) and blocked expression of GADD34 (Fig. 1*J*), one of the proteins known to be overexpressed when eIF2α is phosphorylated. Although SAL alone did not significantly affect [^{35}S]methionine incorporation into nascent proteins, it enhanced the inhibitory effect of α-toxin on [^{35}S]methionine incorporation. SAL also prevented the rebound of [^{35}S]methionine incorporation that was observed at ~3 h after removal of α-toxin (Fig. 1*H*). It was concluded that the inhibitory effect of SAL on metabolic recovery of α-toxin-treated cells was not due to inhibition of translation.

The foregoing results could either reflect a heretofore unknown off-target effect of SAL or, alternatively, a novel role of one of its genuine targets that is not related to the inhibition of translation. Of the two established targets of SAL, GADD34 became detectable only after 2 h of toxin treatment (Fig. 1*J*); in contrast, CReP is constitutively expressed (6). Because SAL-dependent reduction of ATP levels became observable already 45 min after the addition of α-toxin (Fig. 1*D*), we reasoned that KD of CReP might suffice to phenocopy the effect of SAL on ATP levels in α-toxin-treated cells. KD of CReP expression in HaCaT cells was efficient (Fig. 1*K*) and led to increased phosphorylation of eIF2α in toxin-treated cells (Fig. 1*L*). More importantly, it inhibited replenishment of ATP (Fig. 1*M*). Because metabolic recovery of target cells was independent of translation, this suggested that CReP serves a novel function in addition to regulation of translation initiation.

Stress signaling in response to α-toxin, including eIF2α phosphorylation, depends on the efflux of potassium ions (44, 50). Therefore, we tested whether inhibition or ablation of CReP also enhances energy loss in response to PAL, which converts the Na^+/K^+ pump to a channel (51). Neither SAL nor KD of CReP enhanced PAL-dependent ATP loss, although PAL triggered phosphorylation of eIF2α (data not shown). This ruled out the possibility that the adverse effect of SAL or CReP KD on survival of α-toxin-treated cells was due to inhibition of some general function of CReP for energy homeostasis.

CReP but Not PP1c Regulates Uptake of α-Toxin—If not by modulation of translation or through a general effect on energy homeostasis, how could inhibition or ablation of CReP impair metabolic recovery from α-toxin attack? Because we had previously found that endocytosis of α-toxin is vital for metabolic recovery of target cells (25), we wondered whether SAL or KD of CReP might corrupt the traffic machinery required for internalization and neutralization of *S. aureus* α-toxin.

Fluorescence microscopy was employed to glean information on binding and uptake of α-toxin after treatment with SAL. Although SAL did not inhibit binding of fluorescently labeled α-toxin to the PM, juxtanuclear accumulation was attenuated, whereas CHX remained without effect (Fig. 2*A*).

In order to confirm this result by an independent approach and to clarify how far inhibition of uptake also pertained to toxin oligomers, we developed a protocol based on [^{35}S]methionine-labeled α-toxin, surface labeling, and sequential NeutrAvidin pull-down/immunoprecipitation (NP/IP), (Fig. 2*B*). This protocol allowed us to quantify internalization of presumed pore complexes, SDS-stable heptamers (7-mers), and to detect potential changes of uptake in response to any treatments. Accumulation of SDS-resistant 7-mers in cells was markedly suppressed by SAL (Fig. 2*C*). For quantification of this effect, we measured intracellular accumulation of 7-mer between 0.25 h (rather than 0 h because of the late onset of internalization) and 2 h after loading of cells with toxin at 4 °C. Uptake was decreased in the presence of SAL (Fig. 2, *D* and *E*); consistently, more α-toxin remained accessible to surface biotinylation after 2 h at 37 °C (Fig. 2*D*, *left*). In summary, the biochemical approach confirmed the microscopic data and extended them by indicating that SAL inhibits internalization of α-toxin oligomers.

Importantly, KD of CReP expression recapitulated the effect of the inhibitor, SAL, on the formation of juxtanuclear toxin clusters (Fig. 2*F*). In contrast, KD of the catalytic subunit, PP1c, was without effect (Fig. 2*F*). However, KD of PP1c was efficient (Fig. 2*G*) and caused hyperphosphorylation of eIF2α in toxin-treated cells (Fig. 2*H*). In line with the failure of PP1c KD to reduce juxtanuclear accumulation of α-toxin, calyculin A, an inhibitor of PP1c, was also without effect on toxin uptake (data not shown). Consistent with microscopy data, KD of CReP but not of PP1c markedly reduced accumulation of SDS-stable oligomers in cells (Fig. 2, *J* and *K*), whereas they were retained on the surface. This provided conclusive evidence that CReP but not PP1c regulated internalization of α-toxin oligomers.

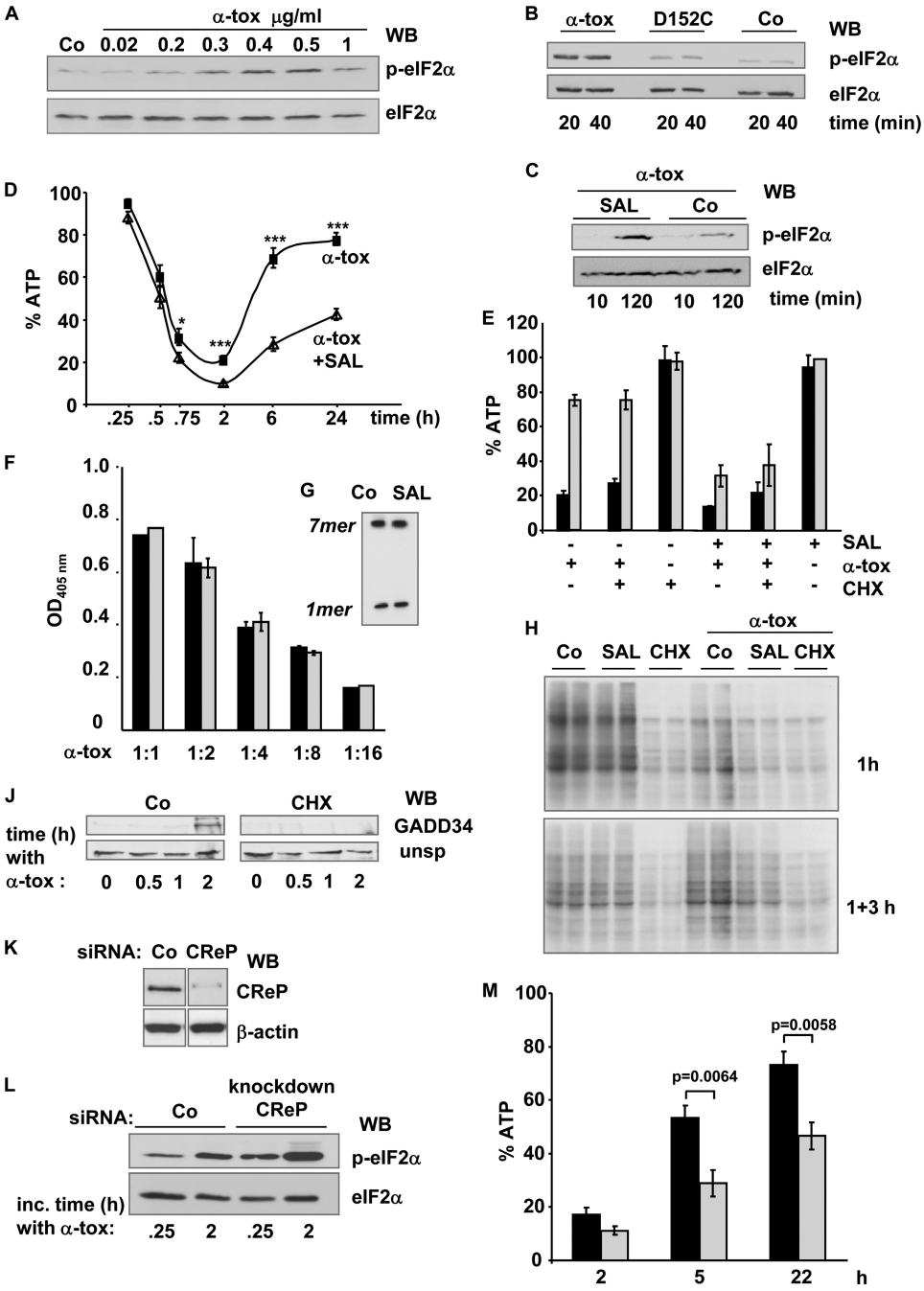

FIGURE 1. **SAL or KD of CReP expression hypersensitizes cells to pore-forming α-toxin**. *A*, Western blot (*WB*) for p-eIF2α and eIF2α in unstressed HaCaT cells (*Co*) or cells treated with different concentrations of α-toxin for 30 min at 37 °C. *B*, Western blot for p-eIF2α and eIF2α with lysates of HaCaT cells treated with wild type α-toxin or mutant D152C (0.5 μg/ml) for the indicated times. *C*, Western blot for p-eIF2α and eIF2α in HaCaT cells treated for the indicated times with α-toxin (0.5 μg/ml) in the presence of SAL (40 μM) or solvent alone (*Co*). *D*, HaCaT cells were pretreated with SAL (*triangles*) or solvent alone (*squares*), loaded with α-toxin (1 μg/ml) in the cold, and incubated at 37 °C with inhibitor/solvent permanently present. After the indicated times, cellular ATP levels (percentage of untreated controls) were determined. *Columns*, mean values; *error bars*, S.E. For comparison of SAL (40 μM) *versus* solvent: *, $n = 9$, $p = 5E\text{-}03$; ***, $n = 14$, p ranging from 2E-04 to 2E-09. *E*, HaCaT cells were pretreated with solvent (−), SAL (40 μM), CHX (10 μg/ml), or a combination of the drugs, loaded with α-toxin (1 μg/ml) in the cold, washed, and incubated at 37 °C in the presence or absence of the drugs. After 2 h (*black columns*) and 6 h (*gray columns*), cellular ATP levels were determined; data represent percentage of untreated controls. *Columns*, mean values; *error bars* S.E.; $n = 3$. *F*, hemolysis assay with serial dilutions of α-toxin (1:1, ~100 ng/ml) in the presence (*gray columns*) or absence (*black columns*) of SAL. *Columns*, mean values; *error bars*, S.E.; $n = 3$. *G*, *red cells* were treated for 30 min with radiolabeled α-toxin (1 μg/ml) in the presence of 40 μM SAL, or solvent (*Co*), lysed, and subjected to IP with anti-α-toxin. Precipitates were analyzed by PAGE/fluorography. *H*, metabolic labeling of cellular proteins with [^{35}S]Met was performed in cells pretreated with SAL, CHX, or solvent alone (*Co*) and subsequently incubated for 1 h in the presence of 100 ng/ml α-toxin (*top gel*) or with α-toxin for 1 h plus 3 h in toxin-free medium (*bottom gel*). Two samples per condition were loaded in adjacent lanes of an SDS-PAGE and analyzed by fluorography. *J*, Western blot analysis of GADD34 following treatment with α-toxin (1 μg/ml), in the presence of CHX or solvent alone (*Co*). *K* and *L*, HaCaT cells were transfected with CReP-siRNA 1 (*CReP*) or scrambled siRNA (*Co*). *K*, transfected cells were analyzed by Western blot for CReP or β-actin; *L*, Western blot for (p-)eIF2α. *M*, cells were transfected with siRNA as in *K* and treated with α-toxin, and ATP was measured at the indicated times. *Black columns*, scrambled siRNA; *gray columns*, CReP-siRNA; *columns* show mean values ± S.E., $n = 5$.

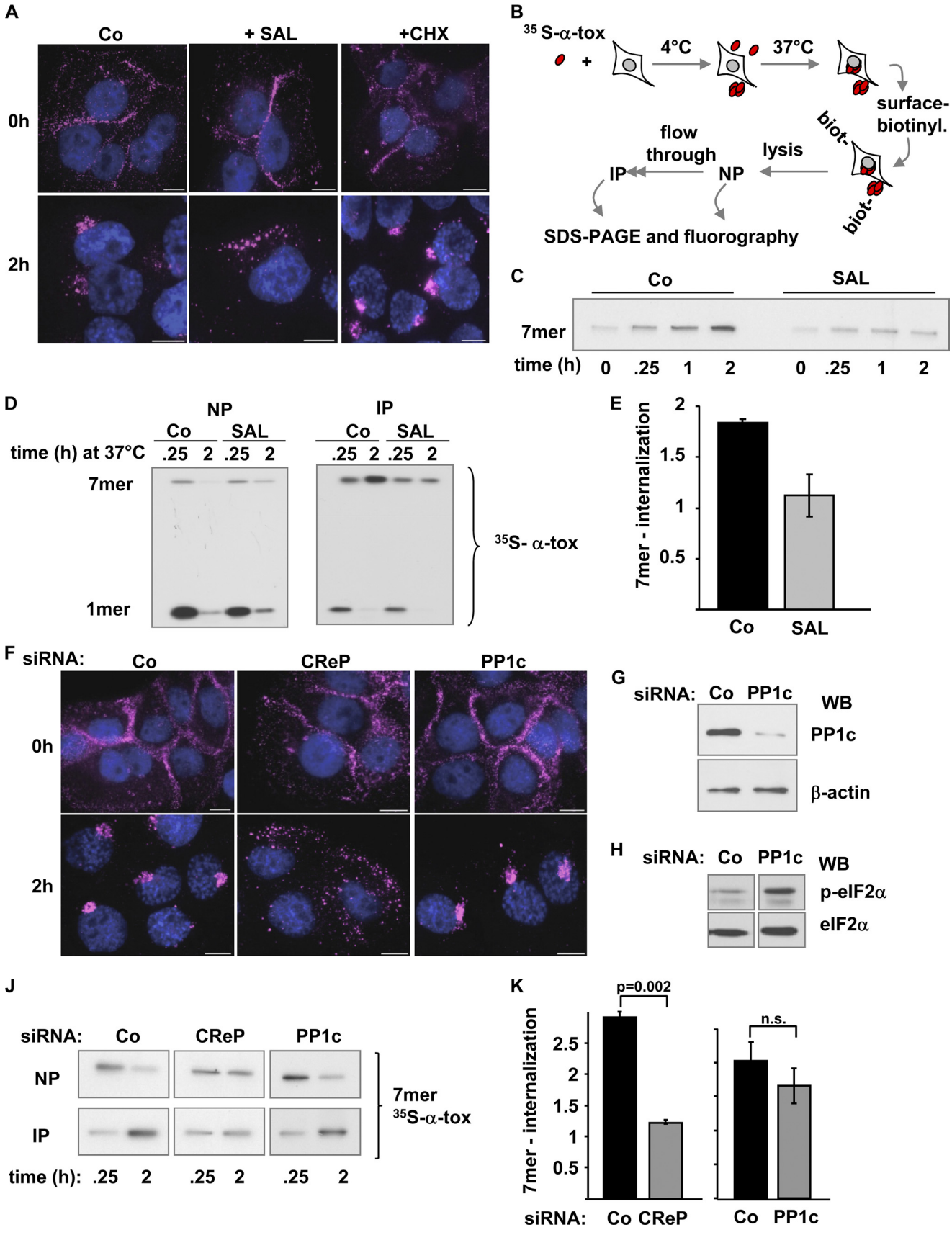
A
Co
+ SAL
+CHX
0h
2h
B
35 S-α-tox
+
4°C
37°C
surface-biotinyl.
biot-
biot-
lysis
NP
IP
flow through
SDS-PAGE and fluorography
C
Co
SAL
7mer
time (h)
0 .25 1 2 0 .25 1 2
D
NP
IP
Co SAL Co SAL
time (h) at 37°C
.25 2 .25 2 .25 2 .25 2
7mer
1mer
35S- α-tox
E
7mer - internalization
2
1.5
1
0.5
Co
SAL
F
siRNA:
Co
CReP
PP1c
0h
2h
G
siRNA: Co PP1c
WB
PP1c
β-actin
H
siRNA: Co PP1c
WB
p-eIF2α
eIF2α
J
siRNA:
Co
CReP
PP1c
NP
IP
7mer
35S-α-tox
time (h):
.25 2 .25 2 .25 2
K
p=0.002
n.s.
7mer - internalization
2.5
2
1.5
1
0.5
siRNA:
Co CReP
Co PP1c

The finding that the inhibitory effect of CReP KD or SAL on uptake of toxin was not replicated by PP1c KD or treatment with calyculin A argued against a role of sustained phosphorylation of eIF2α as the underlying mechanism. This conclusion was confirmed by employing phosphomimetic eIF2α mutant eIF2αS51D (52). Plasmids expressing EGFP-tagged versions of eIF2αS51D or wild-type eIF2α were generated, and uptake of α-toxin was studied by fluorescence microscopy in cells transfected with these constructs. By using metabolic labeling with L-azidohomoalanine and alkyne-based fluorescent labeling of nascent proteins, it was verified that EGFP-tagged eIF2αS51D inhibits the synthesis of proteins in transfected cells (Fig. 3*A*). However, internalization of fluorescently labeled α-toxin was not blocked by EGFP-eIF2αS51D (Fig. 3*B*).

Thus, neither inhibition of translation-initiation nor sustained phosphorylation of eIF2α explained the inhibitory effect of SAL or CReP KD on the internalization of α-toxin. Therefore, the novel role of CReP as a regulator of an endocytic process relied on an unorthodox mode of action, not related to dephosphorylation of eIF2α.

eIF2α and eIF2α Kinases Regulate Uptake of α-Toxin—The finding that the role of CReP in the internalization of α-toxin did not depend on its established mode of action provoked the question of whether the established target of CReP, (p-)eIF2α, was involved at all. Therefore, we assessed uptake of α-toxin following siRNA-mediated KD of eIF2α or eIF2α kinases. KD of eIF2α was verified by Western blot (Fig. 3*C*). Although binding of fluorescently labeled α-toxin to the PM remained unaltered, juxtanuclear accumulation of toxin was reduced by this treatment (Fig. 3*D*). Also, internalization of radiolabeled α-toxin 7-mers was inhibited by KD of eIF2α (Fig. 3, *E* and *F*), and metabolic recovery of the cells was impaired (Fig. 3*G*). Double-KD of GCN2 and PKR, two eIF2α kinases triggered by α-toxin (44), produced an effect similar to KD of eIF2α. GCN2/PKR double-KD (Fig. 3*H*) inhibited toxin-dependent phosphorylation of eIF2α (Fig. 3*J*), and intracellular accumulation of SDS-resistant toxin oligomers was again reduced (Fig. 3, *K* and *L*).

Phospho-eIF2α Is Recruited to the PM of Perforated Cells—To elucidate the role of p-eIF2α in internalization of α-toxin, we wished to employ two-color fluorescence microscopy. The fact that anti-p-eIF2α accurately detects its target in IF applications was demonstrated by a two-pronged approach. HaCaT cells were transfected with EGFP-tagged versions of eIF2α or the non-phosphorylatable mutant eIF2αS51A, immunostained with anti-p-eIF2α, and examined by fluorescence microscopy. Second, Western blot with anti-p-eIF2α was performed following siRNA-mediated KD of eIF2α. The data, summarized in Fig. 4, show that the antibody against p-eIF2α is suitable for IF experiments.

By confocal microscopy, we next compared localization and intensity of p-eIF2α staining in untreated *versus* toxin-treated cells. Untreated HaCaT cells yielded some immunoreactivity of nuclei (Fig. 5*A*); we also noticed nuclear staining in similar IF images of Cos7 or DU-145 cells published earlier (53). When HaCaT cells were treated with α-toxin, p-eIF2α immunoreactive material relocated to the PM (Fig. 5*A*), and fluorescence intensity increased (Fig. 5*B*).

To confirm that p-eIF2α was indeed recruited to the PM and to determine whether this involved physical interaction of p-eIF2α with the PM, we employed cell surface labeling. Cells were treated with a membrane-impermeant biotinylation reagent, and lysates were subjected to NP as outlined in Fig. 5*C*. Recovery of p-eIF2α by NP from lysates of α-toxin-treated cells was selectively increased by surface biotinylation (Fig. 5, *D* and *E*), supporting the notion that p-eIF2α in α-toxin-treated cells associates with the PM.

p-eIF2α and α-Toxin Become Juxtaposed at the PM and Jointly Appear in Early Endosomes—The fact that phosphorylation of eIF2α in toxin-treated cells depends on pore formation and that it associates with the PM in toxin-treated cells raised the possibility that p-eIF2α was formed at or recruited to the site of toxin attack. In order to visualize the spatial relationship of p-eIF2α and α-toxin, cells were briefly incubated with Alexa546-conjugated α-toxin and stained for p-eIF2α. Fluorescence microscopy revealed that the majority of large AlexaFluor546-positive puncta at the PM (plane z2) were juxtaposed to p-eIF2α-positive puncta in planes z2–z6 (Fig. 6*A* and supplemental Movie 1), and overlap even of the total AlexaFluor546 signal in z2 with AlexaFluor488 (p-eIF2α) in z2–z6 was 2.2-fold higher than expected by chance. A similar pattern as in HaCaT was observed in normal human epidermal keratinocytes (data not shown).

Previously, we have shown that α-toxin is endocytosed by epithelial cells (25); and in *Caenorhabditis elegans*, Rab5, a small GTPase involved in endocytosis and homotypic vesicle fusion of early endosomes (54, 55), proved to be important for cellular defenses against small pore-forming toxins (22). Therefore, we wondered whether p-eIF2α might be present in Rab5-positive, early carriers of α-toxin. When cells were transfected with EGFP-tagged Rab5 and treated with Alexa546-α-toxin, numerous puncta double-positive for EGFP-Rab5 and Alexa546-α-toxin were observed under the microscope (Fig. 6*B*). Double-positive puncta were virtually absent from control

FIGURE 2. **CReP regulates uptake of α-toxin.** *A*, cells were treated with SAL (40 μM), CHX (10 μg/ml), or solvent alone (*Co*); loaded with 2 μg/ml AlexaFluor546-labeled α-toxin; and processed for fluorescence microscopy immediately (*top panels*) or after incubation for 2 h at 37 °C (*bottom panels*). *Scale bar*, 10 μm. *B*, scheme of sequential NP/IP for the detection of surface-bound (NP) and internalized (IP) α-toxin. *C*, HaCaT cells were treated with SAL (40 μM) or solvent alone (*Co*) and incubated with radiolabeled α-toxin, and internalized oligomers (7-mers) were recovered by sequential NP/IP followed by PAGE/fluorography (see scheme in Fig. 2*B*). *D*, cells were treated with SAL or solvent alone (*Co*), loaded with 1 μg/ml radiolabeled α-toxin, and analyzed by NP/IP as outlined in the schematic *above* with inhibitors permanently present. *E*, quantitative representation of the effect of SAL as depicted in *D*. 7-mer internalization is defined as internalized 7-mers at 2 h/internalized 7-mers at 0.25 h. *Columns*, mean values; *error bars*, S.E.; $n = 3$. *F*, cells were transfected with control siRNA or with siRNAs targeting CReP or PP1c, treated with 2 μg/ml AlexaFluor546-labeled toxin, and processed for fluorescence microscopy following incubation (*bottom panels*) or not (*top panels*) for 2 h at 37 °C. *Size bars*, 10 μm. *G*, cells were transfected with siRNA targeting PP1c or with control siRNA (*Co*). After 48 h, Western blot (*WB*) for PP1c or β-actin was performed. *H*, Western blot for p-eIF2α and eIF2α after α-toxin treatment (1 μg/ml, 2 h) of cells transfected as described for *G*. *J*, cells were transfected with scrambled siRNA or siRNA targeting CReP or PP1c, loaded with ^{35}S-labeled α-toxin (1 μg/ml), and analyzed by NP/IP after incubation for 0.25 h or 2 h at 37 °C. *K*, bar chart summarizing data from multiple experiments with $n = 7$ for CReP and $n = 3$ for PP1c. *Columns*, mean values; *error bars*, S.E.

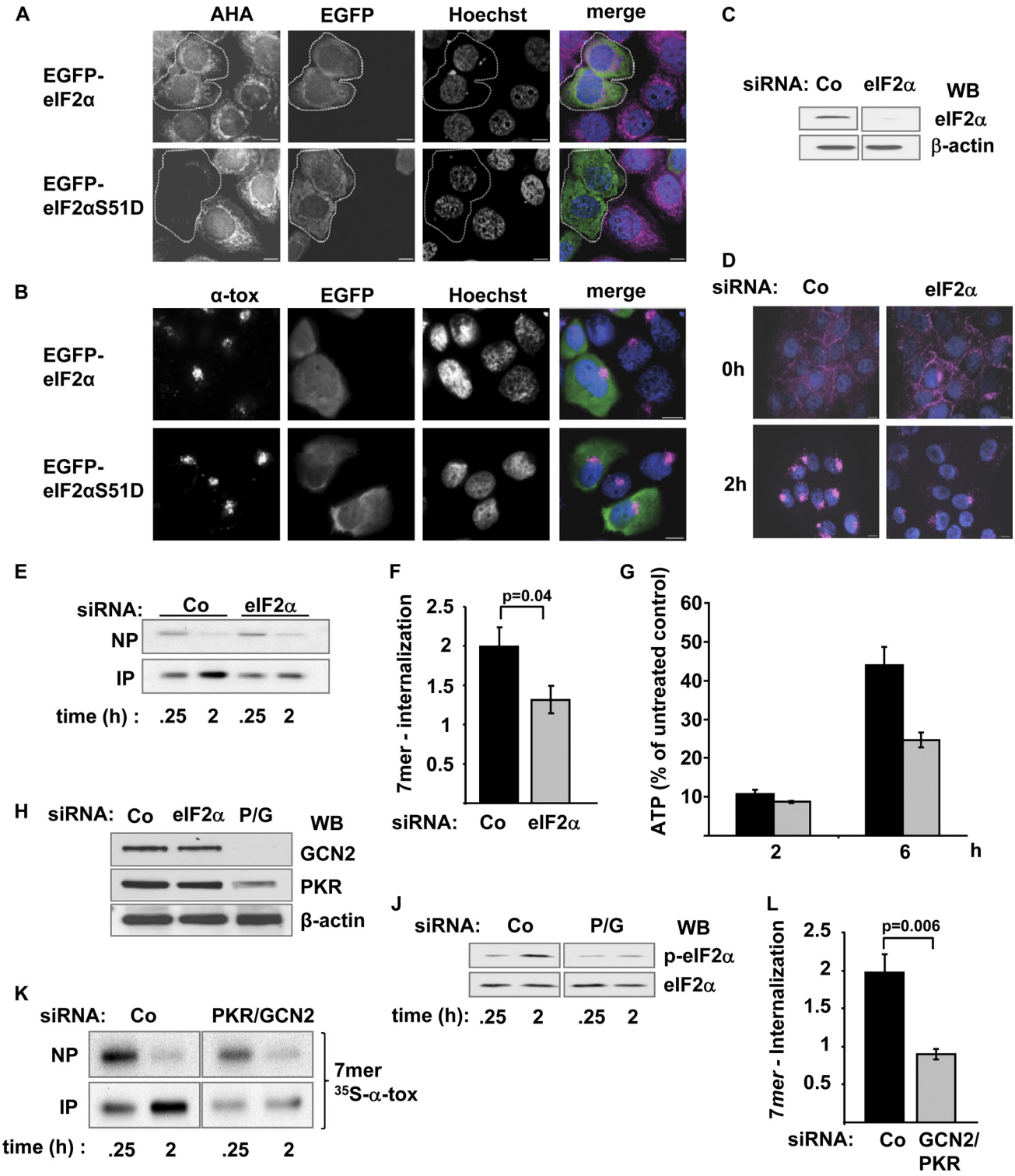

FIGURE 3. **EIF2α and eIF2α kinases, but not inhibition of translation, impact uptake of α-toxin.** *A*, HaCaT cells were transfected with EGFP-eIF2αS51D or EGFP-eIF2α and analyzed for ongoing translation (L-azidohomoalanine incorporation; *magenta* in *merged images*). *B*, HaCaT cells transfected with EGFP-eIF2αS51D or EGFP-eIF2α as in *A* were analyzed for uptake of fluorescently labeled α-toxin (loading with AlexaFluor546-labeled α-toxin (*α-tox*; *magenta* in *merged images*), 2 μg/ml, subsequent incubation for 2 h at 37 °C). *C*, HaCaT cells were transfected with siRNA, targeting eIF2α or control siRNA (*Co*). After 48 h, Western blot (*WB*) was performed to detect eIF2α or β-actin. *D*, cells transfected as in *C* were loaded with 2 μg/ml AlexaFluor546-labeled α-toxin (*magenta*) and processed for fluorescence microscopy immediately (*top panels*) or after 2 h at 37 °C (*bottom panels*). *E*, cells were transfected with the indicated siRNAs, and internalization of 7-mers was analyzed by sequential NP/IP as described in the legend to Fig. 2*B*. *F*, quantification of data from *E*. *Columns*, mean; *error bars*, S.E.; $n = 7$. *G*, HaCaT cells were transfected with control siRNA (*black columns*) or siRNAs targeting eIF2α (*gray columns*), loaded with α-toxin, and incubated for 2 h (*ATP-nadir*), or 6 h (~50% recovery) before cellular ATP content was determined. *Columns*, mean values; *error bars*, S.E.; $n = 3$. *H*, cells were transfected with scrambled siRNA (*Co*) or siRNA targeting eIF2α or co-transfected with a mix of two siRNAs, targeting PKR and GCN2, respectively (*P/G*). Western blot for detection of PKR, GCN2, or β-actin was performed. *J*, cells, transfected with control siRNA or the mix of siRNAs targeting PKR and GCN2, were treated for 0.25 or 2 h with α-toxin (1 μg/ml) and analyzed by Western blot for p-eIF2α and eIF2α. *K*, cells were transfected as in *F*, loaded with radiolabeled α-toxin, and analyzed by NP/IP. *L*, quantification of 7-mer internalization for the experiment shown in *K*; mean values ± S.E., $n = 7$.

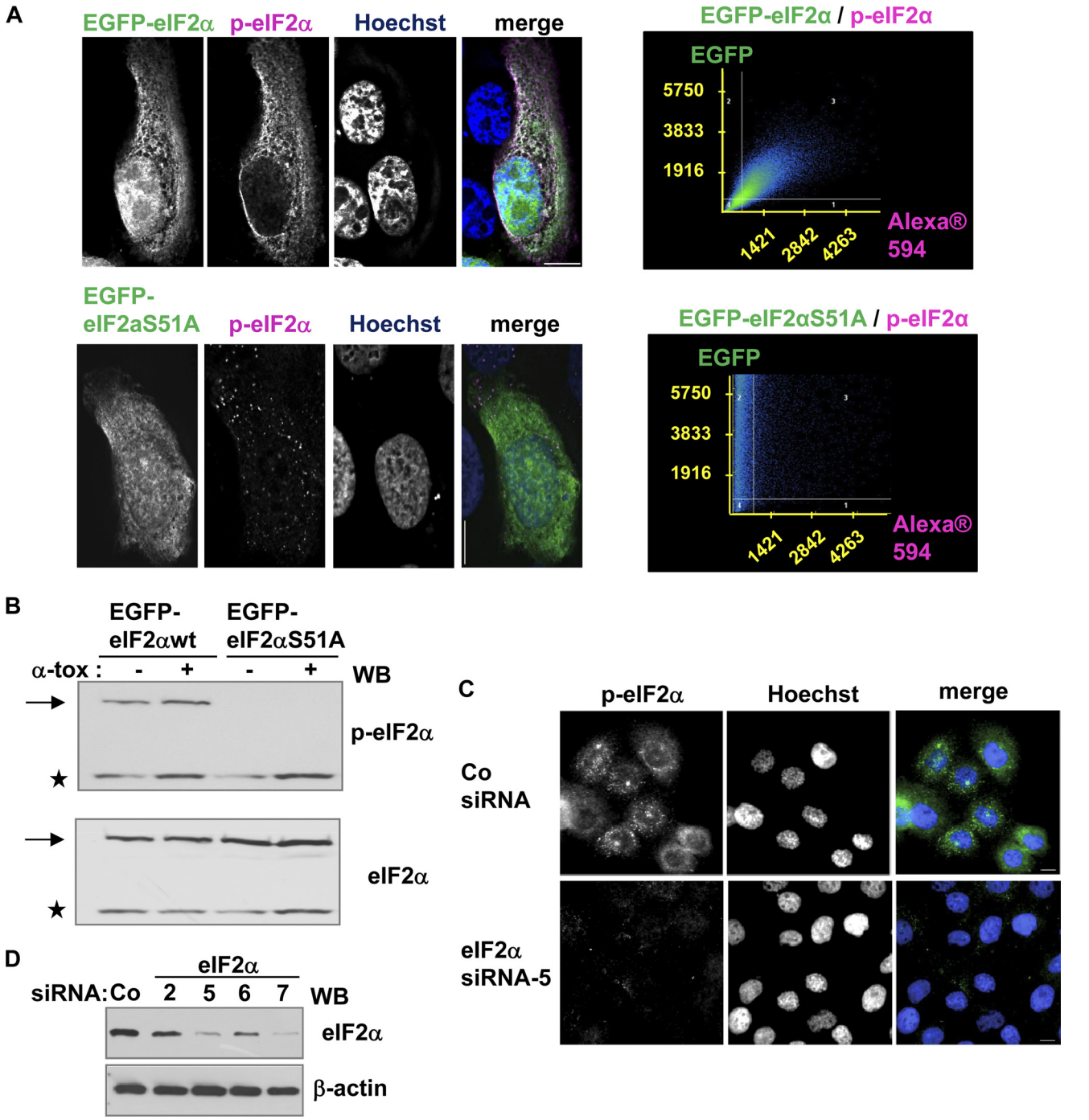

FIGURE 4. **Anti-phospho-eIF2α faithfully detects its target in immunofluorescence experiments.** *A*, HaCaT cells were transfected with pEGFP-eIF2α (*top panels*) or EGFP-eIF2aS51A (*bottom panels*) and immunostained for p-eIF2α with monoclonal rabbit anti-p-eIF2α (*magenta*). *Scale bar*, 10 μm; corresponding *dot plots* on the *right*. *B*, cells, transfected as in *A*, and treated or not with α-toxin (1 μg/ml, 20 min) were analyzed by Western blot with antibodies against (p-)eIF2α. *Asterisks*, endogenous eIF2α; *arrows*, EGFP-fusion proteins. *C*, HaCaT cells were transfected with control siRNA or siRNA targeting eIF2α, treated with α-toxin (1 μg/ml, 20 min), and analyzed for p-eIF2α by IF microscopy. *D*, Western blot of HaCaT cells transfected with various siRNAs targeting eIF2α, as indicated, or control siRNA; the blot was sequentially probed for eIF2α and β-actin.

cells treated with Alexa546-α-toxin-treated cells and immunostained for Nck (Fig. 6*C*). Conjoint presence of α-toxin and p-eIF2α in the membranes of early endosomes was subsequently demonstrated by employing Rab5Q79L, which leads to the formation of enlarged endosomes (56) (Fig. 6*D*). In summary, α-toxin induces focal accumulations of p-eIF2α at the PM, and toxin and p-eIF2α jointly appear in early endosomes.

Interactions between CReP, eIF2α, and α-Toxin—Given the close spatial relationship of p-eIF2α and α-toxin, it appeared likely that the role of CReP for endocytosis of α-toxin, although based on an unorthodox, PP1-c-independent mechanism, involved interaction of CReP with its established target, p-eIF2α. The fact that CReP can interact with phosphorylated eIF2α can seemingly be inferred from the known function of these proteins, but this

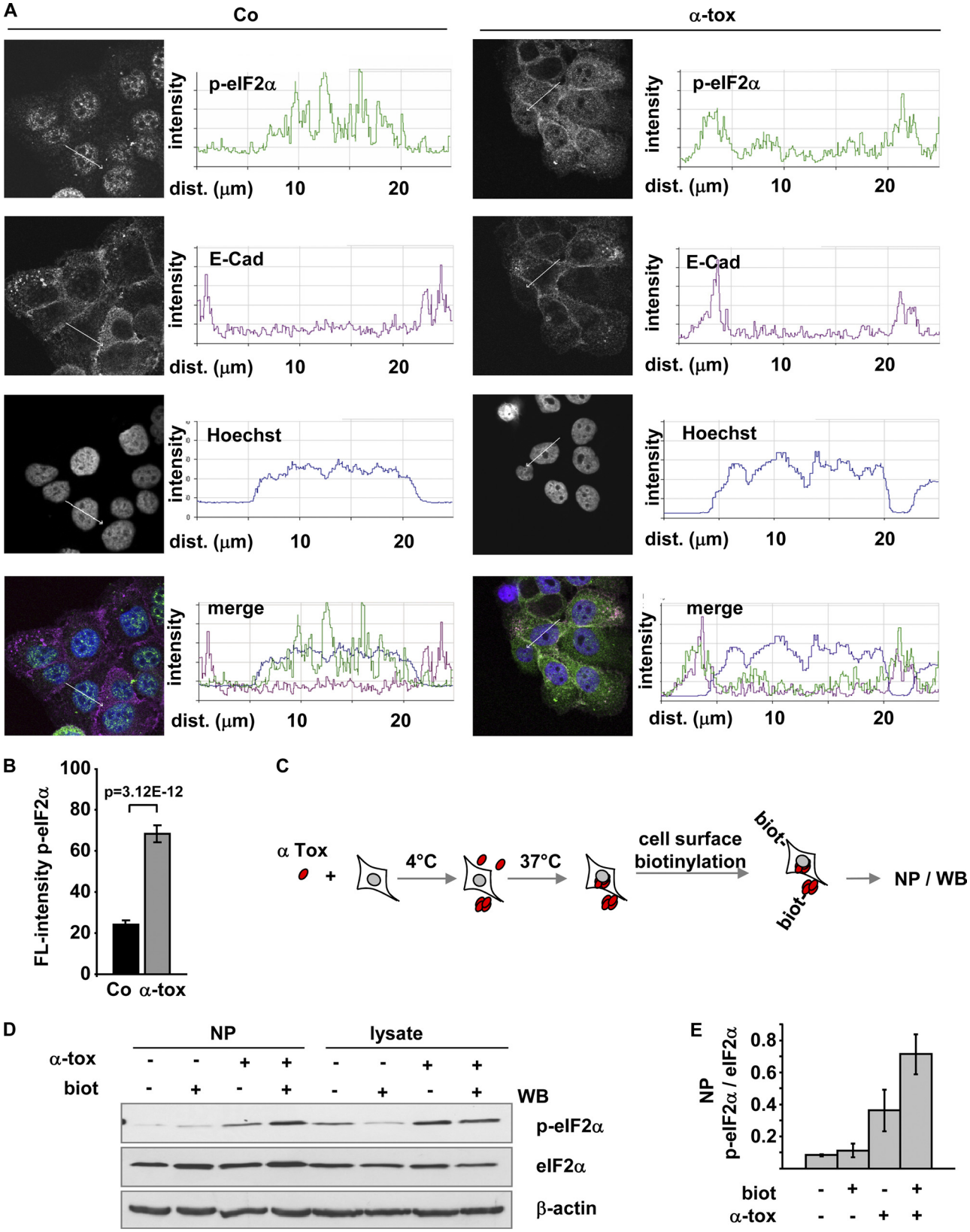

FIGURE 5. **Phospho-eIF2α associates with perforated plasma membrane.** *A*, representative confocal images and corresponding line scan intensity profiles of HaCaT cells, loaded or not (*Co*) with 1 μg/ml α-toxin, subsequently incubated at 37 °C for 30 min, and immunostained for p-eIF2α and E-cadherin (*E-Cad*). *B*, bar chart illustrating the increase of fluorescence (*FL-*) intensity (staining with anti-p-eIF2α; *columns* indicate mean fluorescence intensity (arbitrary units), *error bars* show S.E., $n = 10$ cells) in toxin-treated *versus* untreated cells from a representative experiment. *C*, *scheme* for detection of PM-associated p-eIF2α, as applied below. *D*, cells were loaded or not with α-toxin (1 μg/ml) and incubated at 37 °C for 40 min. Subsequently, cells were surface-biotinylated or not and lysed; lysates were subjected to NP; both lysates and precipitates were analyzed by Western blot (*WB*) for (p-)eIF2α. *E*, band intensities from the NP gels of *D* were measured by densitometry to estimate p-eIF2α/eIF2α associated with the PM. *Columns*, mean values; *error bars*, S.E.; $n = 3$.

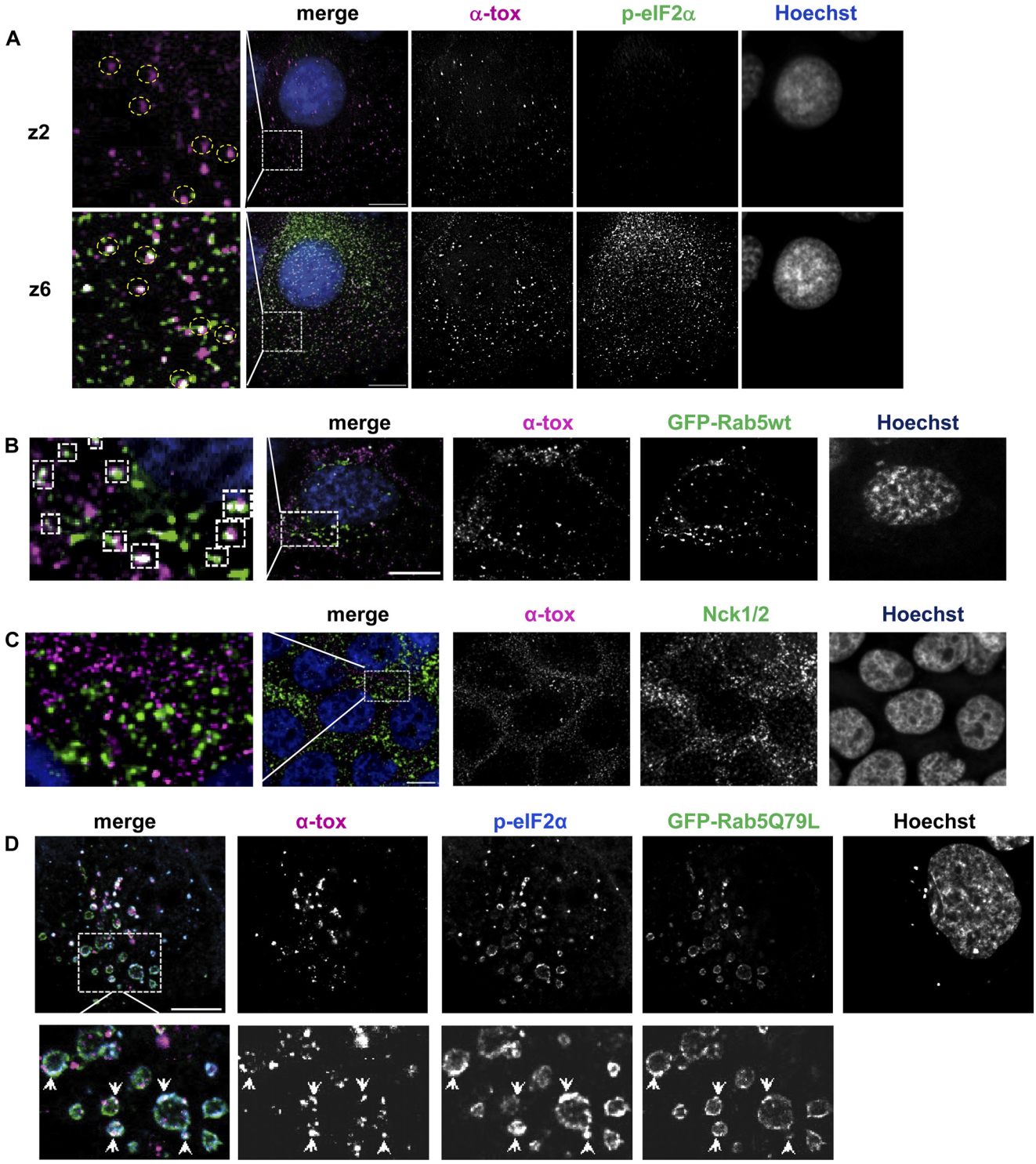

FIGURE 6. **Phospho-eIF2α and α-toxin are juxtaposed at the plasma membrane and jointly appear in early endosomes.** *A*, IF image of HaCaT cells loaded with 2 μg/ml AlexaFluor546-α-toxin (*magenta* in *merged images*), washed, incubated for 20 min at 37 °C, fixed, and immunostained for p-eIF2α (*green*). *Scale bar*, 10 μm; *z2* and *z6* denote focal planes (225 nm/step). *B*, HaCaT cells were transfected with EGFP-Rab5, loaded with 2 μg/ml AlexaFluor546-α-toxin (*magenta*), incubated for 20 min at 37 °C, fixed, stained with Hoechst, and analyzed by deconvolution fluorescence microscopy. *C*, HaCaT cells were loaded with 2 μg/ml AlexaFluor546-labeled α-toxin (*magenta*), washed, incubated for 40 min at 37 °C, fixed, and immunostained for Nck1/2 (*green*). *Scale bar*, 10 μm. *D*, HaCaT cells were transfected with EGFP-Rab5Q79L, loaded with 2 μg/ml AlexaFluor546-α-toxin (*magenta*), incubated for 20 min at 37 °C, fixed, immunostained for p-eIF2α (*green*), and analyzed by fluorescence microscopy.

important detail has actually not been established yet. Because the interaction would be of relevance in the present context, we sought experimental evidence by co-IP. To avoid the potential problem that the presumptive p-eIF2α·CReP complex escapes detection because of rapid dephosphorylation of p-eIF2α, we employed phosphomimetic eIF2αS51D as bait. Cells were transfected with plasmids encoding EGFP-tagged eIF2αS51D, N-terminally EGFP-tagged fusion products of the N- or C-terminal half of eIF2α, or

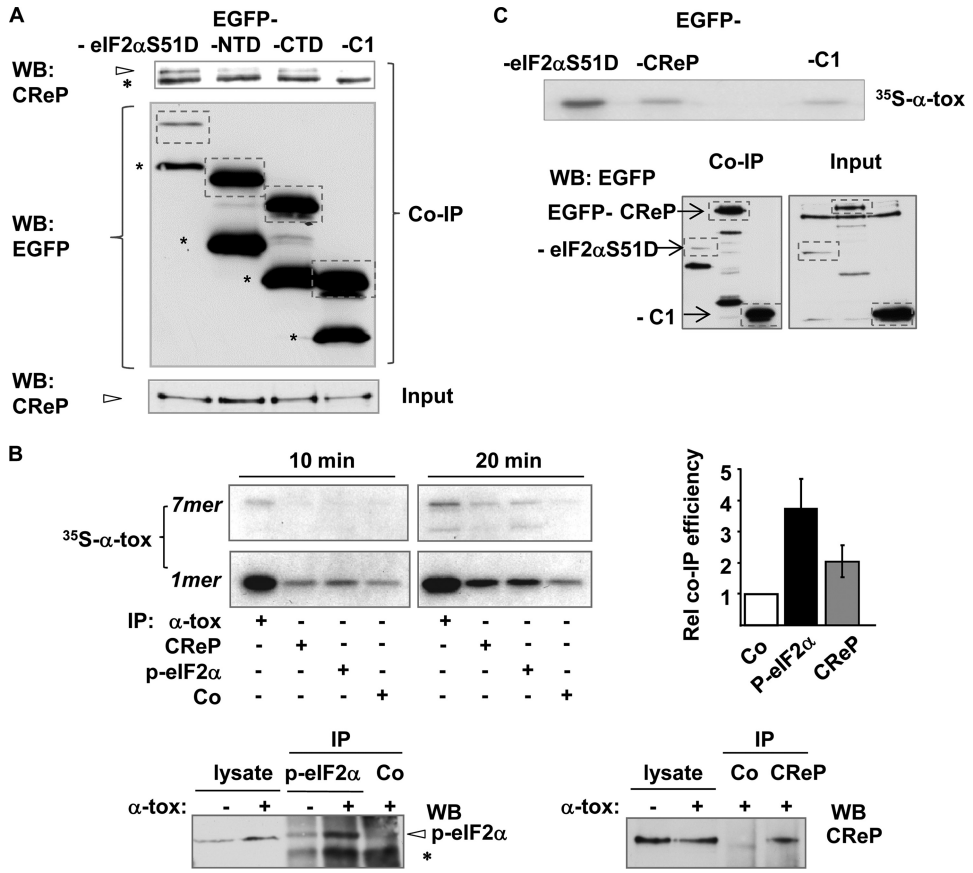

FIGURE 7. **Phospho-eIF2α interacts with α-toxin.** *A*, HaCaT cells were transfected with expression plasmids encoding either EGFP-eIF2αS51D, EGFP-eIF2αS51D-N terminus (*NTD*), EGFP-eIF2α-C terminus (*CTD*), or EGFP alone (*EGFP-C1*). Lysates were obtained and subjected to IP with anti-EGFP-beads; precipitates were separated by SDS-PAGE and analyzed by Western blot (*WB*) for CReP (*top*). *Arrowhead*, CReP; *asterisk*, nonspecific band. *Middle*, Western blot for detection of EGFP (or EGFP fusion products) in precipitates; bands corresponding to full-length EGFP fusion products or EGFP alone are *boxed*; *asterisks* denote break down products. *Bottom*, Western blot for CReP in input lysates. *B*, *top left*, (co-)IP of internally [^{35}S]methionine-labeled α-toxin with antibodies. Cells were loaded with radiolabeled toxin (1 μg/ml), lysed after 10- or 20-min incubation at 37 °C, and subjected to IP using antibodies indicated in the figure. *Co*, anti-GFP. Precipitates were analyzed by SDS-PAGE/fluorography; the bar chart on the *right* shows radioactivity of total [^{35}S]methionine-labeled α-toxin for each sample as measured by scintillation counting. *Columns*, mean values; *error bars*, S.E.; $n = 3$. *Bottom panels*, Western blots for the detection of p-eIF2α (*left*) and CReP (*right*) in lysates or precipitates from experiment shown in the *upper left panels* (20 min samples). *Arrowhead*, p-eIF2α; *asterisk*, a nonspecifically precipitated species that is induced in toxin-treated cells. *C*, HaCaT cells were transfected with plasmids encoding EGFP (*EGFP-C1*) or the fusion products indicated in the figure and loaded with [^{35}S]methionine-radiolabeled α-toxin (1 μg/ml), lysed after 20-min incubation at 37 °C, and subjected to IP with immobilized monoclonal anti-GFP. Precipitates were either analyzed by PAGE/fluorography (*top*) or by Western blot for detection of EGFP (or EGFP fusion proteins) (*bottom left panel*). Western blot for detection of EGFP (or EGFP fusion proteins) in input lysates is shown in the *bottom right panel*. Bands corresponding to full-length products are *boxed*. For maximum recovery of pulled down material, beads were heated to 95 °C for 10 min, thus yielding all of the bound ^{35}S-labeled α-toxin as monomer.

EGFP alone. Lysates of transfected cells were subjected to precipitation with immobilized anti-GFP, and precipitates were analyzed by Western blot for CReP. As shown in Fig. 7*A*, CReP was co-precipitated with tagged, full-length eIF2αS51D, suggesting that intact p-eIF2α will interact with CReP.

To probe for potential direct or indirect physical interactions between toxin and p-eIF2α or CReP, we then performed co-IP experiments with [^{35}S]methionine-labeled α-toxin. Cells were treated with labeled α-toxin for 10 or 20 min, and lysates were subjected to IP with anti-p-eIF2α, anti-CReP, or control antibodies. The precipitate was analyzed by fluorography following separation of proteins by SDS-PAGE. Labeled α-toxin was co-precipitated with anti-p-eIF2α and also with anti-CReP but to a much lesser extent with an irrelevant antibody (anti-EGFP) (Fig. 7*B*). Notably, co-precipitation of α-toxin with anti-p-eIF2α was more efficient when cells were incubated with toxin for 20 min as compared with incubation for 10 min, in line with the kinetics of toxin-dependent eIF2α phosphorylation, thus underscoring the fidelity of this co-IP. In a different co-IP approach, we transfected HaCaT cells with EGFP-tagged eIF2αD, EGFP-CReP, or EGFP alone; incubated these cells with radiolabeled toxin; pulled out the fusion proteins from lysates with immobilized anti-EGFP (eliminating a potential bias due to the use of different antibodies in the first co-IP approach); and visualized the radiolabeled α-toxin co-isolating with EGFP (or EGFP fusion proteins) by fluorography. EGFP recovered small amounts of α-toxin. EGFP-CReP yielded only slightly more, suggesting that the tag might hinder interaction of CReP and toxin. In contrast, EGFP-eIF2αD efficiently co-precipitated α-toxin (Fig. 7*C*), supporting the idea that α-toxin and p-eIF2α may directly or indirectly interact. Expression of the transfected proteins was verified by Western blot (Fig. 7*C*, *bottom*).

Based on the foregoing data, we reasoned that p-eIF2α accumulating at sites of toxin attack could recruit CReP, which in

turn might promote endocytosis of toxin by an unknown, PP1c-independent mechanism. Although low endogenous levels of CReP precluded faithful detection by IF microscopy, transiently transfected FLAG-CReP was found to accumulate next to α-toxin at the PM (supplemental Movie 2).

Endogenous CReP Is Associated with Membranes; Overexpression Induces Vesicles—Although the data of Fig. 2 had shown that CReP regulates uptake of α-toxin, the question remained how CReP could possibly fulfill this unusual function. Because neither PP1c nor translation played a role, two mutually non-exclusive mechanisms were considered. First, CReP could itself impact on budding, scission, or other events required for endocytosis of toxin. Second, CReP could recruit factors endowed with one or more of the required properties.

Few interaction partners of CReP have been identified (57, 58). Among them, we considered the adapter protein Nck to be a potential candidate that could confer CReP-dependent uptake of α-toxin (57) because it also binds to caveolin (59), a known interaction partner of α-toxin (60), and second, because Nck has recently emerged from a large scale analysis (10) as a gene product relevant for defense against small pore-forming toxins in *C. elegans*. However, because we did not detect colocalization of Nck with α-toxin (Fig. 6*C*), we sought alternative explanations for CReP-dependent endocytosis of α-toxin.

Therefore, we asked whether endogenous CReP localizes to membranes. Western blot analysis of differential detergent lysates showed that CReP was actually almost confined to the membrane fraction (Fig. 8*A*). Surface biotinylation, followed by Western blot analysis of Neutravidin-precipitable proteins revealed that CReP membrane association also pertained to the PM (Fig. 8*B*).

Next, we examined cells transiently overexpressing CReP by IF microscopy. Strikingly, transfected cells contained numerous vesicles decorated with CReP (Fig. 8*C*). These vesicles were not an artifact due to fixation or permeabilization, because fluorescence microscopy of unfixed, unpermeabilized cells, transfected with an N-terminally EGFP-tagged version of CReP, yielded the same result (Fig. 8*D*).

Delineation of CReP N-terminal Vesicle Induction/Accumulation Region—Truncation analysis revealed that the N-terminal-most 140 amino acids of CReP are both necessary and sufficient to confer upon EGFP the ability to associate with vesicles (Fig. 8, *D–F*); C-terminal truncations retained this phenotype, whereas it was lost in EGFP-CReP(140–720) (Fig. 8*D*). In control cells expressing EGFP alone; nuclei and cytoplasm were diffusely stained; no fluorescent vesicles were discerned (Fig. 8*E*). Using differential interference contrast optics, we found that expression of EGFP-CReP(1–140) not only labeled intracellular vesicles but significantly increased the number of vesicles per cell, as compared with EGFP alone (Fig. 8, *E–H*).

The amino acid sequence of the CReP N terminus is highly conserved (Fig. 9*A*). Analysis with the algorithm of Petersen *et al.* (61) predicted an amphipathic α-helix (Fig. 9*B*). Consistent with the fact that the N terminus is distal from (and unrelated to) the PP1c interaction domain of CReP, silencing of PP1c did not prevent decoration of vesicles with EGFP-CReP(1–140) (Fig. 9*C*). Deletion of the α-helix almost abolished vesicle induction, although EGFP-CReP(1–140)Δαhelix appears to retain the ability to associate with membranes because it tended to accumulate in the cell periphery (Fig. 9*D*). In summary, the CReP N terminus confers association with and induction of vesicles; therefore, we term the domain spanning amino acids 1–140 the CReP N-terminal vesicle induction/accumulation region.

Intralumenal Accumulation of N-Rh-PE in Vesicles Decorated with CReP (VDC)—Although overexpressed (EGFP-)CReP induced and decorated vesicles, it was also present in reticular structures, reminiscent of the ER. Cotransfection of EGFP-CReP or EGFP-CReP(1–140) and DSRed-ER revealed significant overlap (Fig. 10*A*), but some VDC were devoid of the ER marker (supplemental Movies 3 and 4).

Because the diameter of VDC was similar to that of MVB (~0.5 μm) and because a subpopulation of MVB may be derived from the ER (62), we studied the distribution of N-Rh-PE, a fluorescent lipid marker of intralumenal vesicles of multivesicular bodies and of exosomes, in cells expressing EGFP-CReP. Intriguingly, N-Rh-PE accumulated in the lumen of VDC (Fig. 10*B*).

A Role of CReP for Exocytosis from Erythroleukemia Cells—The above finding prompted us to investigate whether CReP might impact exocytosis. Because it would be difficult to distinguish a potential inhibitory effect of CReP KD on exocytosis of α-toxin from the inhibitory effect of CReP KD on toxin internalization, we chose another experimental system for this purpose. The human erythroleukemia cell line K562 has provided important insights into exocytosis and into the role of MVB in this process (63–66). Levels of acetylcholinesterase (AChE) released by K562 cells via exosomes can be conveniently quantified by a colorimetric assay. We transfected K562 cells with scrambled siRNA or siRNAs targeting CReP or PP1c and confirmed knockdown by Western blots (Fig. 10*C*). Exosome preparations from cells treated with siRNAs targeting CReP contained significantly lower AChE activity (Fig 10*D*) and also lower amounts of AChE protein (Fig. 10*E*) as compared with control cells or cells treated with siRNAs targeting PP1c, although AChE in lysates was even increased in CReP KD cells (Fig. 10*E*). Similarly, actin (another regular constituent of exosomes) was decreased in the exosome preparation but not in lysates of CReP KD cells. This suggested that exocytosis in K562 cells was under the control of CReP.

If this was because CReP aided fusion of MVB with the PM, KD of CReP would be expected to also inhibit recycling of internalized membrane receptors, like transferrin receptors (TrfR), and thus lower the abundance of receptor molecules on the cell surface. On the contrary, if CReP promoted exocytosis by generally increasing inward budding at endosomal membranes, KD of CReP would be expected to reduce exosomal release of TrfR from cells so that levels of total TrfR and/or TrfR on the cell surface might even increase. Expression of TrfR was not changed after ablation of CReP (Fig. 8*E*), but the abundance of TrfR on the cell surface was significantly lowered (Fig. 10*F*). Therefore, a role of CReP in MVB/PM fusion would seem more likely than a role in inward budding; other mechanisms may also play a role. At any rate, the data confirmed that CReP impacts membrane traffic.

DISCUSSION

The present study uncovers a role of PPP1R15B/CReP in membrane traffic. Surprisingly, this does not rely on PP1c or the established function of CReP as a regulatory subunit of eIF2α-phosphatase. The novel role of CReP surfaced when we studied cell-autonomous defenses against α-toxin, a structurally well characterized small pore-forming toxin, which is thought to be of great significance for the pathogenesis of diseases caused by *S. aureus*. The role of CReP in membrane traffic was further substantiated by the observation of CReP-dependent vesiculation and CReP-dependent exocytosis from erythroleukemia cells, two additional PP1c-independent functions.

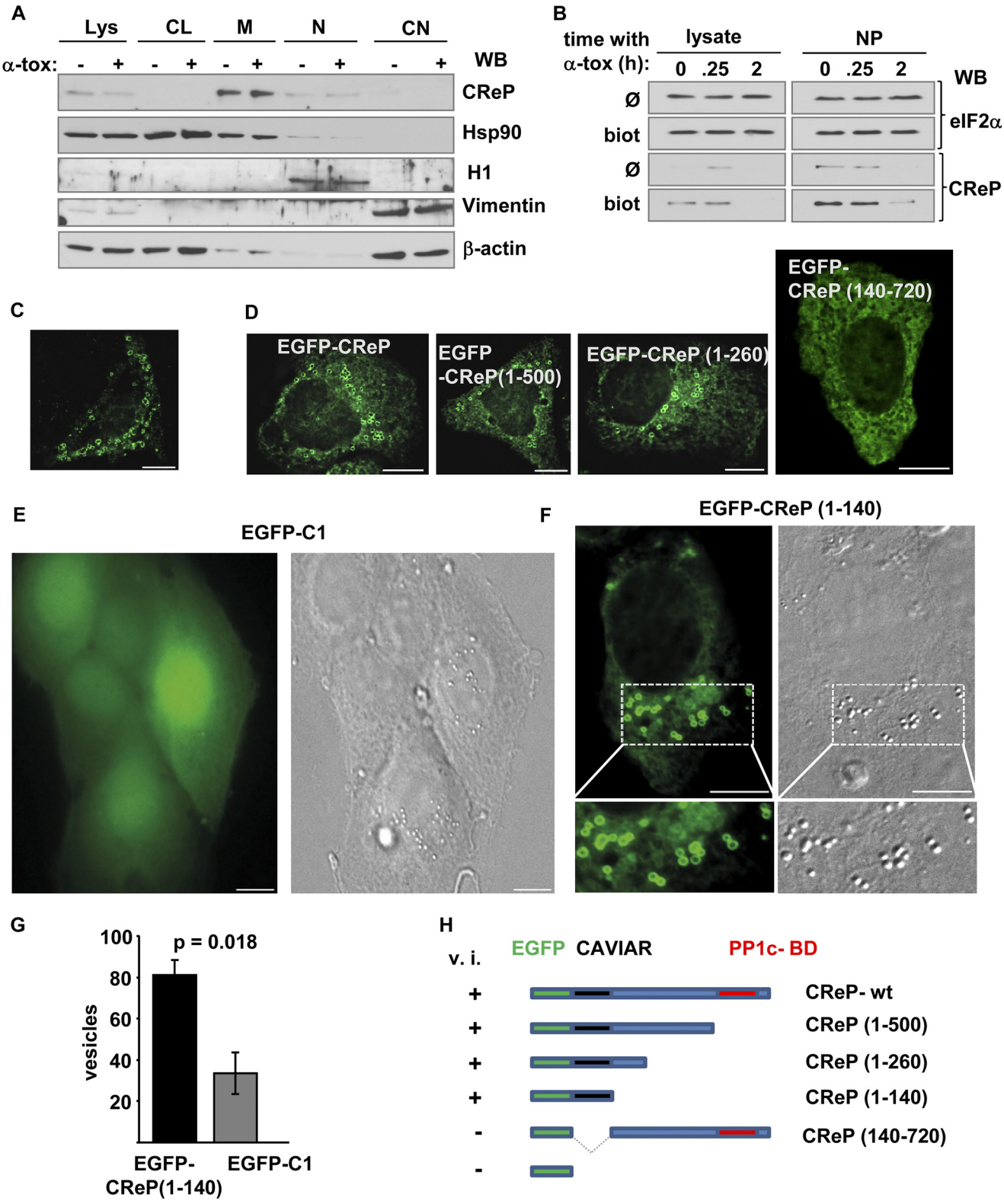

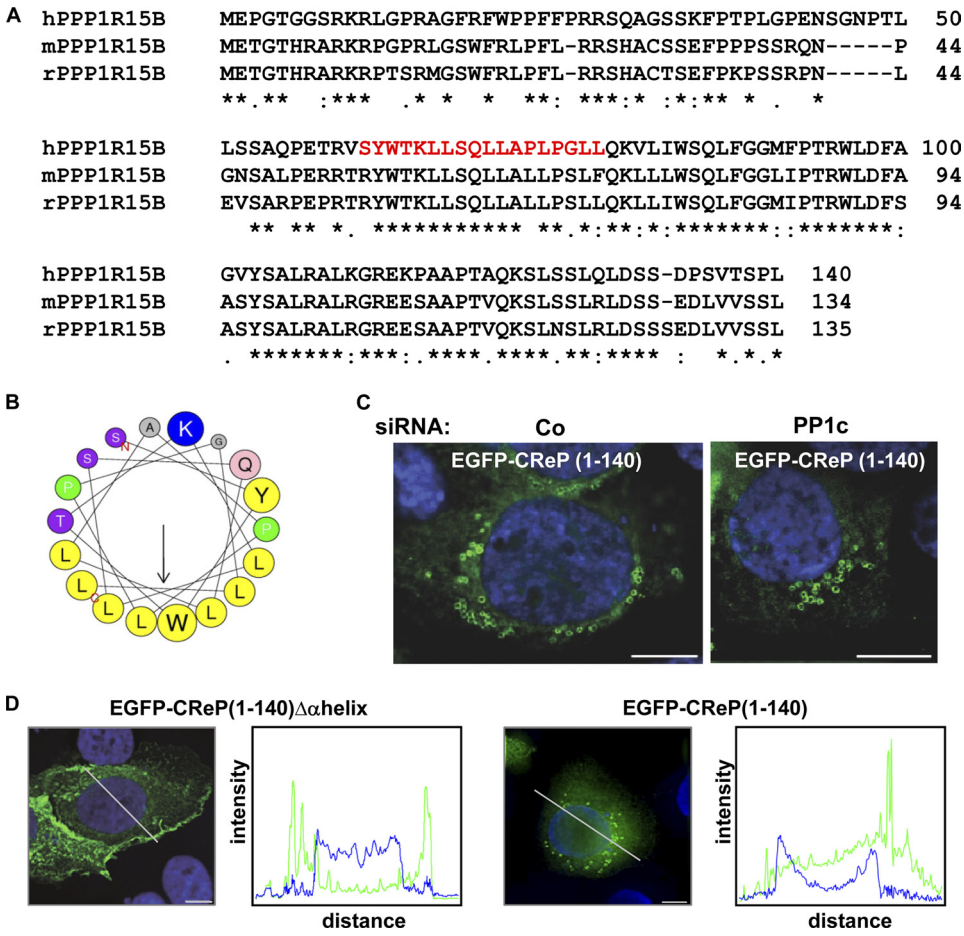

FIGURE 9. **A predicted amphipathic α-helix in the CReP N terminus confers association with vesicles.** *A*, alignment of amino acid sequences of N termini of human, mouse, or rat PPP1r15B/CReP. *Asterisks*, amino acid identity in all three species. *Red color* indicates sequence shown in the helical wheel plot representation in *B*. *B*, helical wheel plot of amino acids 61–78 of human CReP, revealing a short, amphipathic α-helix. *Yellow*, non-polar residues. *C*, HaCaT cells were transfected with control siRNA or siRNA targeting PP1c and with plasmid EGFP-CReP(1–140). KD of PP1c was verified by Western blot (see Fig. 2*G*). Transfected cells were analyzed by fluorescence microscopy. *D*, HaCaT cells, transfected with EGFP-CReP(1–140)$\Delta\alpha$-helix or EGFP-CReP(1–140), were analyzed by IF microscopy. *Size bar*, 10 μm. Fluorescence intensity profiles correspond to line scans indicated by the *white lines* in photographs; *green*, EGFP; *blue*, Hoechst. Note the single peak corresponding to a juxtanuclear vesicle in the scan of EGFP-CReP(1–140)-transfected cells.

The data, summarized in Fig. 10*G*, add unexpected twists to the emerging picture of an intricate relationship between translation and traffic. Previous studies had shown that membrane stress inflicted by mutations in *sec* or *end* genes in yeast or by chlorpromazine in mammalian cells elicits phosphorylation of eIF2α (67, 68). Not only do PFT too trigger phosphorylation of eIF2α (44), but as shown here, the archaic stress response is exploited to promote the removal of pores by endocytosis. Recently, mTORC1, a master regulator of translation, has been found to control endocytosis (69–71). However, in contrast to mTORC1, CReP and (p-)eIF2α appear not to impact endocytosis by regulating translation. Rather, the traffic machinery co-opts these proteins. This may offer critical advantages for target cells of PFT; like translation, traffic involves highly energy-consuming processes (72). As shown here and in previous work (35, 73), translation is dispensable during the acute phase of membrane repair, but membrane traffic is vital (22, 24, 25). Not only would down-regulation of translation initiation next to membrane lesions conserve local ATP supplies required for timely removal of pores, but p-eIF2α itself could be exploited for the uptake process. The observed juxtaposition of p-eIF2α to clusters of membrane-bound toxin, the conjoint presence of

FIGURE 8. **CReP is associated with and impacts on cellular membranes.** *A*, HaCaT cells, treated or not with α-toxin (200 ng/ml) for 30 min at 37 °C, were subjected to sequential detergent lysis, and the various lysates were analyzed by Western blot (*WB*) for CReP or subcellular marker proteins (*Lys*, complete lysate; *CL*, cytosol; *M*, membranes; *N*, nucleus; *CN*, cytoskeleton). *B*, neutravidin pull-down after surface biotinlyation of α-toxin-treated HaCaT cells was performed as in Fig. 5*C*; precipitates were analyzed by Western blot for CReP and for eIF2α as a control. Note the loss of CReP in the 2 h sample, due to short half-life of CReP and global translational stop in the presence of toxin. *C*, cells were transfected with CReP and analyzed by IF microscopy. *Size bar*, 10 μm. *D–F*, HaCaT cells were transfected with expression plasmids encoding the indicated products. Cells were imaged by fluorescence microscopy; representative images are shown. Note fluorescent vesicles in all images but EGFP-C1 control (*E*) and the N-terminal deletion construct EGFP-CReP(140–720) (*D*). Representative IF and corresponding differential interference contrast images of cells transfected with EGFP-C1 (expressing EGFP alone) are shown in *E*, and images of cells transfected with EGFP-CReP(1–140) are shown in *F*. *G*, cells were transfected with EGFP or EGFP-CReP(1–140), and vesicles discernable by differential interference contrast were counted at day 1 post-transfection in green fluorescent cells; *numbers* are vesicles per field (*columns*, mean; *error bars*, S.E.; $n = 4$ experiments; $\geq$8 fields/experiment). *H*, summary of results from IF experiments with various fusion constructs comprising truncations of CReP. *v.i.*, vesicle induction as observed in *C*; *CAVIAR*, CReP vesicle induction/association region.

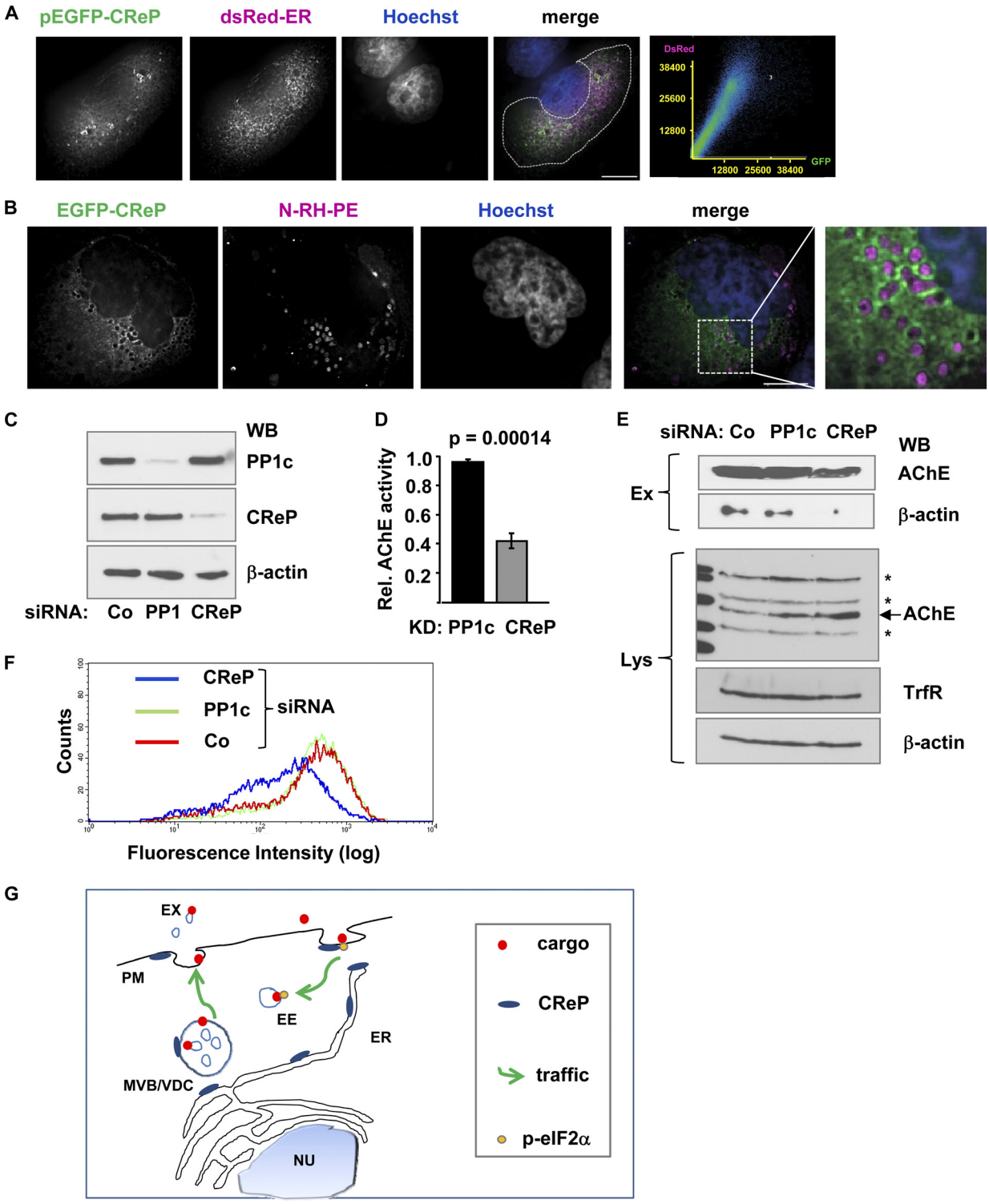

FIGURE 10. **CReP regulates retrograde membrane traffic.** *A*, HaCaT cells were cotransfected with pEGFP-CReP and dsRed-ER and analyzed by fluorescence microscopy. Staining patterns with the two markers showed spatial overlap (see supplemental Movie 3 for complete *z*-stack) and correlation of intensities. Pearson's correlation coefficient was 0.60 ± 0.03 (mean ± S.E.; $n = 10$ cells from a representative experiment). *B*, cells were transfected with pEGFP-CReP, loaded for 1 h with N-Rh-PE on ice, incubated for 2.5 h at 37 °C, and analyzed by fluorescence microscopy. *C*, K562 cells were transfected with control siRNA or siRNAs targeting CReP or PP1c. Western blot was performed, and the membrane was sequentially probed as indicated. *D*, exosomes were prepared from supernatants collected from K562 cells, transfected as in *C*, and AChE activity was measured; data were normalized for activity in samples receiving control siRNA (equal to 1). *Columns*, mean values; *error bars*, S.E.; $n = 4$. *E*, exosome preparations (*Ex*) from *D* and corresponding whole cell lysates (*Lys*) were analyzed by Western blot (*WB*) with the indicated antibodies. *F*, cells were transfected with siRNAs as in *C* and analyzed by flow cytometry for surface expression of TrfR (CD71); fluorescence intensity (median channel) in cells treated with CReP-siRNA *versus* Co-siRNA was 367 ± 51 and 196 ± 12, respectively (mean ± S.E., $n = 3$). *G*, model of CReP effect on membrane traffic. CReP localizes to cellular membranes, including ER and PM. Upon local accumulation of CReP or in response to additional cues, CReP would impact membrane curvature. This may occur, for instance, when CReP is recruited to foci of p-eIF2α, marking membrane lesions inflicted by α-toxin. Similarly, local changes of CReP concentrations at endogenous membranes may impact retrograde traffic. *NU*, nucleus; *EE*, early endosomes.

toxin and p-eIF2α in early endosomes, and the reduced uptake following KD of p-eIF2α all imply that p-eIF2α is indeed important for uptake of α-toxin. The importance of spatial organization of signals emanating from the PM and the role of signaling foci has recently been highlighted (74). That traffic and translation are spatially coordinated is further suggested by the observation that the trypanosomal eIF2α kinase TbeIF2K1 is located at the flagellar pocket (75), the exclusive site of endocytosis and exocytosis in that organism. In retrospect, it seems that our experimental paradigm was well suited to uncover the role of CReP and eIF2α for endocytosis, because α-toxin served as both a traceable cargo and a trigger of eIF2α phosphorylation.

S. aureus colonizes mucosa or skin of a large fraction of the human population, and this organism may cause life-threatening disease even in the immunocompetent (76). α-Toxin is expressed by the majority of clinical isolates of *S. aureus* and is a major secreted virulence factor of this bacterium. Signaling pathways have been shaped by the co-evolution of hosts and pathogens (77). It is conceivable that the selective pressure exerted by α-toxin may have driven evolution of a dedicated defense mechanism involving CReP-dependent uptake of this toxin, but similar, non-canonical roles of CReP in traffic may also play a role for handling of other cargo, including some other PFT. We propose that the role of p-eIF2α during CReP-dependent uptake is to mark sites of membrane attack. Synopsis of the following results supports this concept: p-eIF2α accumulated at sites of toxin binding to the PM; second, phosphorylation of eIF2α in response to toxin depends on membrane perforation; and third, p-eIF2α interacts with α-toxin in co-IP experiments. Straightforwardly, CReP would then be recruited to its target, p-eIF2α, accumulating next to membrane lesions. That p-eIF2α was shown to interact with both toxin and CReP in co-IP experiments supported this concept.

The effect of CReP on constitutive exocytosis in erythroleukemia cells indicated that CReP is of broader significance for membrane traffic. Because reduction of membrane tension by non-secretory exocytosis of internal membranes is critical for endocytosis (78), the finding also provides an alternative mechanistic explanation for the role of CReP in endocytosis of α-toxin. Of note, both endo- and exocytosis have been implicated in the response to PFT (22, 24, 25). The fact that CReP associates with membranes, including the PM, and upon overexpression induces and decorates intracellular vesicles is compatible with a direct involvement of CReP in membrane traffic, not ruling out the possibility that CReP recruits proteins that affect membrane curvature or other relevant parameters/events.

Although CReP has not been linked to membrane traffic before, its association with membranes has been noted in a recent paper focusing on PPP1r15A/GADD34 (79), which was published as the present work was in progress. Regarding membrane association of CReP, our data extend the observations of Zhou *et al.* (79) by showing that endogenous CReP associates with both the ER and the PM; second, that as in the case of GADD34, an N-terminal amphipathic α-helix confers ER localization of CReP; and third, that overexpressed CReP induces and decorates vesicles. Notably, overexpression of GADD34 leads to distension of the ER, but vesicle induction was not reported. ER localization of both CReP and GADD34 appears to be at least in part determined by amphipathic α-helices in their N termini. However, the overall sequences of the N termini of CReP and GADD34 and also of the α-helices responsible for ER localization share no significant homology, in keeping with the different effects of the two PPP1r15 proteins on ER morphology.

Short amphipathic α-helices have been implicated in the generation of membrane curvature and budding (80–85). In line with this, vesicle induction by EGFP-CReP(1–140) depended on a short amphipathic α-helix within the N terminus. That vesicle induction required neither PP1c nor the putative PP1c-binding domain of CReP is compatible with the idea that the vesiculation phenomenon relates to the role of CReP in endocytosis of α-toxin, because this too was independent of PP1c.

Few publications on PPP1r15B/CReP are available in the literature. One study based on gene knock-out in mice provided important information on the role of CReP *in vivo*. Although one conclusion from these experiments was that CReP acts in a rather linear fashion during murine development (CReP modulates the phosphorylation of eIF2α, and this regulates translation initiation), homozygosity for $eIF2\alpha^{S51A}$ did not efficiently rescue the fetal anemia phenotype observed in CReP knock-out mice (4). In light of the present findings, and considering the importance of exocytosis for maturation of reticulocytes, this failure of $eIF2\alpha^{S51A}$ to fully rescue anemia may actually reflect functions of CReP *in vivo*, related to those uncovered here *in vitro*.

To conclude, PPP1r15B/CReP impacts membrane traffic by a PP1c-independent mechanism. To the best of our knowledge, this represents the first example of co-option of regulators of translation initiation by the traffic machinery.

Acknowledgments—We thank H. Bayley for plasmids, Gilles Spoden for helpful discussions and reagents, Jens Stieler for help with microscopy applications, and Monika Wiedmann for help with preparation of the manuscript.

REFERENCES

1. Harding, H. P., Novoa, I., Zhang, Y., Zeng, H., Wek, R., Schapira, M., and Ron, D. (2000) Regulated translation initiation controls stress-induced gene expression in mammalian cells. *Mol. Cell* **6,** 1099–1108
2. Wek, R. C., Jiang, H. Y., and Anthony, T. G. (2006) Coping with stress. eIF2 kinases and translational control. *Biochem. Soc. Trans.* **34,** 7–11
3. Kojima, E., Takeuchi, A., Haneda, M., Yagi, A., Hasegawa, T., Yamaki, K., Takeda, K., Akira, S., Shimokata, K., and Isobe, K. (2003) The function of GADD34 is a recovery from a shutoff of protein synthesis induced by ER stress. Elucidation by GADD34-deficient mice. *FASEB J.* **17,** 1573–1575
4. Harding, H. P., Zhang, Y., Scheuner, D., Chen, J. J., Kaufman, R. J., and Ron, D. (2009) Ppp1r15 gene knockout reveals an essential role for translation initiation factor 2 α (eIF2α) dephosphorylation in mammalian development. *Proc. Natl. Acad. Sci. U.S.A.* **106,** 1832–1837
5. Boyce, M., Bryant, K. F., Jousse, C., Long, K., Harding, H. P., Scheuner, D., Kaufman, R. J., Ma, D., Coen, D. M., Ron, D., and Yuan, J. (2005) A selective inhibitor of eIF2α dephosphorylation protects cells from ER stress. *Science* **307,** 935–939
6. Jousse, C., Oyadomari, S., Novoa, I., Lu, P., Zhang, Y., Harding, H. P., and

Ron, D. (2003) Inhibition of a constitutive translation initiation factor 2α phosphatase, CReP, promotes survival of stressed cells. *J. Cell Biol.* **163,** 767–775
7. Scheuner, D., Patel, R., Wang, F., Lee, K., Kumar, K., Wu, J., Nilsson, A., Karin, M., and Kaufman, R. J. (2006) Double-stranded RNA-dependent protein kinase phosphorylation of the α-subunit of eukaryotic translation initiation factor 2 mediates apoptosis. *J. Biol. Chem.* **281,** 21458–21468
8. Bellier, A., Chen, C. S., Kao, C. Y., Cinar, H. N., and Aroian, R. V. (2009) Hypoxia and the hypoxic response pathway protect against pore-forming toxins in *C. elegans*. *PLoS Pathog.* **5,** e1000689
9. Chen, C. S., Bellier, A., Kao, C. Y., Yang, Y. L., Chen, H. D., Los, F. C., and Aroian, R. V. (2010) WWP-1 is a novel modulator of the DAF-2 insulin-like signaling network involved in pore-forming toxin cellular defenses in *Caenorhabditis elegans*. *PLoS One* **5,** e9494
10. Kao, C. Y., Los, F. C., Huffman, D. L., Wachi, S., Kloft, N., Husmann, M., Karabrahimi, V., Schwartz, J. L., Bellier, A., Ha, C., Sagong, Y., Fan, H., Ghosh, P., Hsieh, M., Hsu, C. S., Chen, L., and Aroian, R. V. (2011) Global functional analyses of cellular responses to pore-forming toxins. *PLoS Pathog.* **7,** e1001314
11. Gurcel, L., Abrami, L., Girardin, S., Tschopp, J., and van der Goot, F. G. (2006) Caspase-1 activation of lipid metabolic pathways in response to bacterial pore-forming toxins promotes cell survival. *Cell* **126,** 1135–1145
12. Huffman, D. L., Abrami, L., Sasik, R., Corbeil, J., van der Goot, F. G., and Aroian, R. V. (2004) Mitogen-activated protein kinase pathways defend against bacterial pore-forming toxins. *Proc. Natl. Acad. Sci. U.S.A.* **101,** 10995–11000
13. Husmann, M., Dersch, K., Bobkiewicz, W., Beckmann, E., Veerachato, G., and Bhakdi, S. (2006) Differential role of p38 mitogen-activated protein kinase for cellular recovery from attack by pore-forming *S. aureus* α-toxin or streptolysin O. *Biochem. Biophys. Res. Commun.* **344,** 1128–1134
14. Babiychuk, E. B., Monastyrskaya, K., Potez, S., and Draeger, A. (2009) Intracellular Ca^{2+} operates a switch between repair and lysis of streptolysin O-perforated cells. *Cell Death Differ.* **16,** 1126–1134
15. Draeger, A., Monastyrskaya, K., and Babiychuk, E. B. (2011) Plasma membrane repair and cellular damage control. The annexin survival kit. *Biochem. Pharmacol.* **81,** 703–712
16. Saka, H. A., Gutiérrez, M. G., Bocco, J. L., and Colombo, M. I. (2007) The autophagic pathway. A cell survival strategy against the bacterial pore-forming toxin *Vibrio cholerae* cytolysin. *Autophagy* **3,** 363–365
17. Gutierrez, M. G., Saka, H. A., Chinen, I., Zoppino, F. C., Yoshimori, T., Bocco, J. L., and Colombo, M. I. (2007) Protective role of autophagy against *Vibrio cholerae* cytolysin, a pore-forming toxin from *V. cholerae*. *Proc. Natl. Acad. Sci. U.S.A.* **104,** 1829–1834
18. Aroian, R., and van der Goot, F. G. (2007) Pore-forming toxins and cellular non-immune defenses (CNIDs). *Curr. Opin. Microbiol.* **10,** 57–61
19. Freche, B., Reig, N., and van der Goot, F. G. (2007) The role of the inflammasome in cellular responses to toxins and bacterial effectors. *Semin. Immunopathol.* **29,** 249–260
20. Gonzalez, M. R., Bischofberger, M., Pernot, L., van der Goot, F. G., and Frêche, B. (2008) Bacterial pore-forming toxins. The (w)hole story? *Cell Mol. Life Sci.* **65,** 493–507
21. Bischofberger, M., Gonzalez, M. R., and van der Goot, F. G. (2009) Membrane injury by pore-forming proteins. *Curr. Opin. Cell Biol.* **21,** 589–595
22. Los, F. C., Kao, C. Y., Smitham, J., McDonald, K. L., Ha, C., Peixoto, C. A., and Aroian, R. V. (2011) RAB-5- and RAB-11-dependent vesicle-trafficking pathways are required for plasma membrane repair after attack by bacterial pore-forming toxin. *Cell Host Microbe* **9,** 147–157
23. Keyel, P. A., Loultcheva, L., Roth, R., Salter, R. D., Watkins, S. C., Yokoyama, W. M., and Heuser, J. E. (2011) Streptolysin O clearance through sequestration into blebs that bud passively from the plasma membrane. *J. Cell Sci.* **124,** 2414–2423
24. Idone, V., Tam, C., Goss, J. W., Toomre, D., Pypaert, M., and Andrews, N. W. (2008) Repair of injured plasma membrane by rapid Ca^{2+}-dependent endocytosis. *J. Cell Biol.* **180,** 905–914
25. Husmann, M., Beckmann, E., Boller, K., Kloft, N., Tenzer, S., Bobkiewicz, W., Neukirch, C., Bayley, H., and Bhakdi, S. (2009) Elimination of a bacterial pore-forming toxin by sequential endocytosis and exocytosis. *FEBS Lett.* **583,** 337–344
26. Keefe, D., Shi, L., Feske, S., Massol, R., Navarro, F., Kirchhausen, T., and Lieberman, J. (2005) Perforin triggers a plasma membrane repair response that facilitates CTL induction of apoptosis. *Immunity* **23,** 249–262
27. Thiery, J., Keefe, D., Saffarian, S., Martinvalet, D., Walch, M., Boucrot, E., Kirchhausen, T., and Lieberman, J. (2010) Perforin activates clathrin- and dynamin-dependent endocytosis, which is required for plasma membrane repair and delivery of granzyme B for granzyme-mediated apoptosis. *Blood* **115,** 1582–1593
28. Moskovich, O., and Fishelson, Z. (2007) Live cell imaging of outward and inward vesiculation induced by the complement c5b-9 complex. *J. Biol. Chem.* **282,** 29977–29986
29. Pilzer, D., and Fishelson, Z. (2005) Mortalin/GRP75 promotes release of membrane vesicles from immune attacked cells and protection from complement-mediated lysis. *Int. Immunol.* **17,** 1239–1248
30. Pilzer, D., Gasser, O., Moskovich, O., Schifferli, J. A., and Fishelson, Z. (2005) Emission of membrane vesicles. Roles in complement resistance, immunity, and cancer. *Springer Semin. Immunopathol.* **27,** 375–387
31. McNeil, P. L., and Steinhardt, R. A. (1997) Loss, restoration, and maintenance of plasma membrane integrity. *J. Cell Biol.* **137,** 1–4
32. Terasaki, M., Miyake, K., and McNeil, P. L. (1997) Large plasma membrane disruptions are rapidly resealed by Ca^{2+}-dependent vesicle-vesicle fusion events. *J. Cell Biol.* **139,** 63–74
33. McNeil, P. L., and Kirchhausen, T. (2005) An emergency response team for membrane repair. *Nat. Rev. Mol. Cell Biol.* **6,** 499–505
34. McNeil, P. L., and Steinhardt, R. A. (2003) Plasma membrane disruption. Repair, prevention, adaptation. *Annu. Rev. Cell Dev. Biol.* **19,** 697–731
35. Gonzalez, M. R., Bischofberger, M., Frêche, B., Ho, S., Parton, R. G., and van der Goot, F. G. (2011) Pore-forming toxins induce multiple cellular responses promoting survival. *Cell Microbiol.* **13,** 1026–1043
36. Bubeck Wardenburg, J., Bae, T., Otto, M., Deleo, F. R., and Schneewind, O. (2007) Poring over pores. α-Hemolysin and Panton-Valentine leukocidin in *Staphylococcus aureus* pneumonia. *Nat. Med.* **13,** 1405–1406
37. Bhakdi, S., and Tranum-Jensen, J. (1991) α-Toxin of *Staphylococcus aureus*. *Microbiol. Rev.* **55,** 733–751
38. Song, L., Hobaugh, M. R., Shustak, C., Cheley, S., Bayley, H., and Gouaux, J. E. (1996) Structure of staphylococcal α-hemolysin, a heptameric transmembrane pore. *Science* **274,** 1859–1866
39. Liang, X., and Ji, Y. (2006) α-Toxin interferes with integrin-mediated adhesion and internalization of *Staphylococcus aureus* by epithelial cells. *Cell Microbiol.* **8,** 1656–1668
40. Pany, S., and Krishnasastry, M. V. (2007) Aromatic residues of caveolin-1 binding motif of α-hemolysin are essential for membrane penetration. *Biochem. Biophys. Res. Commun.* **363,** 197–202
41. Valeva, A., Hellmann, N., Walev, I., Strand, D., Plate, M., Boukhallouk, F., Brack, A., Hanada, K., Decker, H., and Bhakdi, S. (2006) Evidence that clustered phosphocholine headgroups serve as sites for binding and assembly of an oligomeric protein pore. *J. Biol. Chem.* **281,** 26014–26021
42. Wilke, G. A., and Bubeck Wardenburg, J. (2010) Role of A disintegrin and metalloprotease 10 in *Staphylococcus aureus* α-hemolysin-mediated cellular injury. *Proc. Natl. Acad. Sci. U.S.A.* **107,** 13473–13478
43. Walker, B., and Bayley, H. (1995) Key residues for membrane binding, oligomerization, and pore forming activity of staphylococcal α-hemolysin identified by cysteine scanning mutagenesis and targeted chemical modification. *J. Biol. Chem.* **270,** 23065–23071
44. Kloft, N., Neukirch, C., Bobkiewicz, W., Veerachato, G., Busch, T., von Hoven, G., Boller, K., and Husmann, M. (2010) Pro-autophagic signal induction by bacterial pore-forming toxins. *Med. Microbiol. Immunol.* **199,** 299–309
45. Boukamp, P., Petrussevska, R. T., Breitkreutz, D., Hornung, J., Markham, A., and Fusenig, N. E. (1988) Normal keratinization in a spontaneously immortalized aneuploid human keratinocyte cell line. *J. Cell Biol.* **106,** 761–771
46. Haugwitz, U., Bobkiewicz, W., Han, S. R., Beckmann, E., Veerachato, G., Shaid, S., Biehl, S., Dersch, K., Bhakdi, S., and Husmann, M. (2006) Pore-forming *Staphylococcus aureus* α-toxin triggers epidermal growth factor receptor-dependent proliferation. *Cell Microbiol.* **8,** 1591–1600
47. Deng, J., Harding, H. P., Raught, B., Gingras, A. C., Berlanga, J. J., Scheuner, D., Kaufman, R. J., Ron, D., and Sonenberg, N. (2002) Activation of GCN2

in UV-irradiated cells inhibits translation. *Curr. Biol.* **12,** 1279–1286
48. Dieterich, D. C., Link, A. J., Graumann, J., Tirrell, D. A., and Schuman, E. M. (2006) Selective identification of newly synthesized proteins in mammalian cells using bioorthogonal noncanonical amino acid tagging (BONCAT). *Proc. Natl. Acad. Sci. U.S.A.* **103,** 9482–9487
49. Cantin, R., Diou, J., Bélanger, D., Tremblay, A. M., and Gilbert, C. (2008) Discrimination between exosomes and HIV-1. Purification of both vesicles from cell-free supernatants. *J. Immunol. Methods* **338,** 21–30
50. Kloft, N., Busch, T., Neukirch, C., Weis, S., Boukhallouk, F., Bobkiewicz, W., Cibis, I., Bhakdi, S., and Husmann, M. (2009) Pore-forming toxins activate MAPK p38 by causing loss of cellular potassium. *Biochem. Biophys. Res. Commun.* **385,** 503–506
51. Wu, C. H. (2009) Palytoxin. Membrane mechanisms of action. *Toxicon* **54,** 1183–1189
52. Scheuner, D., Song, B., McEwen, E., Liu, C., Laybutt, R., Gillespie, P., Saunders, T., Bonner-Weir, S., and Kaufman, R. J. (2001) Translational control is required for the unfolded protein response and *in vivo* glucose homeostasis. *Mol. Cell* **7,** 1165–1176
53. Kedersha, N., Chen, S., Gilks, N., Li, W., Miller, I. J., Stahl, J., and Anderson, P. (2002) Evidence that ternary complex (eIF2-GTP-$tRNA_i^{Met}$)-deficient preinitiation complexes are core constituents of mammalian stress granules. *Mol. Biol. Cell* **13,** 195–210
54. Stenmark, H. (2009) Rab GTPases as coordinators of vesicle traffic. *Nat. Rev. Mol. Cell Biol.* **10,** 513–525
55. Huotari, J., and Helenius, A. (2011) Endosome maturation. *EMBO J.* **30,** 3481–3500
56. Stenmark, H., Parton, R. G., Steele-Mortimer, O., Lütcke, A., Gruenberg, J., and Zerial, M. (1994) Inhibition of rab5 GTPase activity stimulates membrane fusion in endocytosis. *EMBO J.* **13,** 1287–1296
57. Latreille, M., and Larose, L. (2006) Nck in a complex containing the catalytic subunit of protein phosphatase 1 regulates eukaryotic initiation factor 2α signaling and cell survival to endoplasmic reticulum stress. *J. Biol. Chem.* **281,** 26633–26644
58. Taylor, R. C., Acquaah-Mensah, G., Singhal, M., Malhotra, D., and Biswal, S. (2008) Network inference algorithms elucidate Nrf2 regulation of mouse lung oxidative stress. *PLoS Comput. Biol.* **4,** e1000166
59. Lee, H., Park, D. S., Wang, X. B., Scherer, P. E., Schwartz, P. E., and Lisanti, M. P. (2002) Src-induced phosphorylation of caveolin-2 on tyrosine 19. Phospho-caveolin-2 ($Tyr(P)^{19}$) is localized near focal adhesions, remains associated with lipid rafts/caveolae, but no longer forms a high molecular mass hetero-oligomer with caveolin-1. *J. Biol. Chem.* **277,** 34556–34567
60. Pany, S., Vijayvargia, R., and Krishnasastry, M. V. (2004) Caveolin-1 binding motif of α-hemolysin. Its role in stability and pore formation. *Biochem. Biophys. Res. Commun.* **322,** 29–36
61. Petersen, B., Petersen, T. N., Andersen, P., Nielsen, M., and Lundegaard, C. (2009) A generic method for assignment of reliability scores applied to solvent accessibility predictions. *BMC Struct. Biol.* **9,** 51
62. Anteunis, A. (1974) Origin and fate of the multivesicular bodies in PHA-stimulated lymphocytes. *Cell Tissue Res.* **149,** 497–511
63. Johnstone, R. M., Adam, M., Hammond, J. R., Orr, L., and Turbide, C. (1987) Vesicle formation during reticulocyte maturation. Association of plasma membrane activities with released vesicles (exosomes). *J. Biol. Chem.* **262,** 9412–9420
64. Vidal, M., Mangeat, P., and Hoekstra, D. (1997) Aggregation reroutes molecules from a recycling to a vesicle-mediated secretion pathway during reticulocyte maturation. *J. Cell Sci.* **110,** 1867–1877
65. Savina, A., Vidal, M., and Colombo, M. I. (2002) The exosome pathway in K562 cells is regulated by Rab11. *J. Cell Sci.* **115,** 2505–2515
66. Fader, C. M., Sánchez, D., Furlán, M., and Colombo, M. I. (2008) Induction of autophagy promotes fusion of multivesicular bodies with autophagic vacuoles in k562 cells. *Traffic* **9,** 230–250
67. Deloche, O., de la Cruz, J., Kressler, D., Doère, M., and Linder, P. (2004) A membrane transport defect leads to a rapid attenuation of translation initiation in Saccharomyces cerevisiae. *Mol. Cell* **13,** 357–366
68. De Filippi, L., Fournier, M., Cameroni, E., Linder, P., De Virgilio, C., Foti, M., and Deloche, O. (2007) Membrane stress is coupled to a rapid translational control of gene expression in chlorpromazine-treated cells. *Curr. Genet.* **52,** 171–185
69. Hennig, K. M., Colombani, J., and Neufeld, T. P. (2006) TOR coordinates bulk and targeted endocytosis in the *Drosophila melanogaster* fat body to regulate cell growth. *J. Cell Biol.* **173,** 963–974
70. MacGurn, J. A., Hsu, P. C., Smolka, M. B., and Emr, S. D. (2011) TORC1 regulates endocytosis via Npr1-mediated phosphoinhibition of a ubiquitin ligase adaptor. *Cell* **147,** 1104–1117
71. Peña-Llopis, S., Vega-Rubin-de-Celis, S., Schwartz, J. C., Wolff, N. C., Tran, T. A., Zou, L., Xie, X. J., Corey, D. R., and Brugarolas, J. (2011) Regulation of TFEB and V-ATPases by mTORC1. *EMBO J.* **30,** 3242–3258
72. Soldati, T., and Schliwa, M. (2006) Powering membrane traffic in endocytosis and recycling. *Nat. Rev. Mol. Cell Biol.* **7,** 897–908
73. Valeva, A., Walev, I., Gerber, A., Klein, J., Palmer, M., and Bhakdi, S. (2000) Staphylococcal α-toxin. Repair of a calcium-impermeable pore in the target cell membrane. *Mol. Microbiol.* **36,** 467–476
74. Bethani, I., Skånland, S. S., Dikic, I., and Acker-Palmer, A. (2010) Spatial organization of transmembrane receptor signaling. *EMBO J.* **29,** 2677–2688
75. Moraes, M. C., Jesus, T. C., Hashimoto, N. N., Dey, M., Schwartz, K. J., Alves, V. S., Avila, C. C., Bangs, J. D., Dever, T. E., Schenkman, S., and Castilho, B. A. (2007) Novel membrane-bound eIF2α kinase in the flagellar pocket of *Trypanosoma brucei*. *Eukaryot. Cell* **6,** 1979–1991
76. van Belkum, A., Melles, D. C., Nouwen, J., van Leeuwen, W. B., van Wamel, W., Vos, M. C., Wertheim, H. F., and Verbrugh, H. A. (2009) Co-evolutionary aspects of human colonization and infection by *Staphylococcus aureus*. *Infect. Genet. Evol.* **9,** 32–47
77. Münter, S., Way, M., and Frischknecht, F. (2006) Signaling during pathogen infection. *Science's STKE 2006*, re5
78. Apodaca, G. (2002) Modulation of membrane traffic by mechanical stimuli. *Am. J. Physiol. Renal Physiol.* **282,** F179–F190
79. Zhou, W., Brush, M. H., Choy, M. S., and Shenolikar, S. (2011) Association with endoplasmic reticulum promotes proteasomal degradation of GADD34 protein. *J. Biol. Chem.* **286,** 21687–21696
80. Lee, M. C., Orci, L., Hamamoto, S., Futai, E., Ravazzola, M., and Schekman, R. (2005) Sar1p N-terminal helix initiates membrane curvature and completes the fission of a COPII vesicle. *Cell* **122,** 605–617
81. Gallop, J. L., Jao, C. C., Kent, H. M., Butler, P. J., Evans, P. R., Langen, R., and McMahon, H. T. (2006) Mechanism of endophilin N-BAR domain-mediated membrane curvature. *EMBO J.* **25,** 2898–2910
82. Ford, M. G., Mills, I. G., Peter, B. J., Vallis, Y., Praefcke, G. J., Evans, P. R., and McMahon, H. T. (2002) Curvature of clathrin-coated pits driven by epsin. *Nature* **419,** 361–366
83. Hurley, J. H., Boura, E., Carlson, L. A., and Różycki, B. (2010) Membrane budding. *Cell* **143,** 875–887
84. Graham, T. R., and Kozlov, M. M. (2010) Interplay of proteins and lipids in generating membrane curvature. *Curr. Opin. Cell Biol.* **22,** 430–436
85. Sens, P., Johannes, L., and Bassereau, P. (2008) Biophysical approaches to protein-induced membrane deformations in trafficking. *Curr. Opin. Cell Biol.* **20,** 476–482